Available online at www.sciencedirect.com
SCIENCE DIRECT®
Journal of Marine Systems 38 (2003) 221–257
JOURNAL OF MARINE SYSTEMS
www.elsevier.com/locate/jmarsys

An eddy-permitting, coupled ecosystem-circulation model of the Arabian Sea: comparison with observations

Michio Kawamiya*, Andreas Oschlies[1]

Institut für Meereskunde an der Universität Kiel, Düsternbrooker Weg 20, D-24105, Kiel, Germany

Received 20 September 2001; accepted 24 September 2002

Abstract

A nitrogen-based, pelagic ecosystem model has been coupled with an eddy-permitting ocean general circulation model of the Arabian Sea, and the results are compared with observations. The seasonal variability simulated by the model is in good agreement with observations: during the southwest monsoon season, phytoplankton increases in the western Arabian Sea due to upwelling along the coast; during the northeast monsoon season, phytoplankton abundance is large in the northern Arabian Sea because of the enhanced nitrate entrained by relatively deep vertical mixing. Two major differences are, however, found in the basin-wide comparison between model results and observations: an unrealistic nitrate maximum in the subsurface layer of the northern Arabian Sea and too low primary production in oligotrophic regimes. The former may be attributed to the lack of denitrification in the model. Possible causes for the latter include the present model's underestimation of fast nutrient recycling, the neglect of carbon fixation decoupled from nitrogen uptake and of nitrogen fixation, and inadequate nitrate entrainment by mixed layer deepening. The rate at which simulated nitrate increases in the northern Arabian Sea is 11–24 TgN/year, and should correspond to the denitrification rate integrated over the northern Arabian Sea assuming that the loss of nitrogen through denitrification is balanced by advective input. The model does not reproduce the observed phytoplankton bloom in the late southwest monsoon season. Possible causes are that the mixed layer may be too shallow in summer and that the horizontal transport of nitrate from the coast of Oman may be too weak. Sensitivity experiments demonstrate a strong dependence of the simulated primary productivity on the vertical mixing scheme and on the inclusion of a fast recycling loop in the ecosystem model.

Keywords: Ecosystem; Eddy-permitting; Arabian Sea; Monsoon; Modeling; Denitrification

1. Introduction

The distinct seasonality in physics and biology in the Arabian Sea provides scientists such a unique field that it inspired them to conduct a number of observational programs under the framework of the Joint Global Ocean Flux Study (JGOFS), which aims at quantifying biogeochemical fluxes in the ocean with a particular emphasis on carbon (cf., Smith et al., 1998).

* Corresponding author. Present address: Integrated Modelling Research Program, Frontier Research System for Global Change, 3173-25, Showa-machi, 236-0001, Kanazawa, Yokohama, Japan. Fax: +81-45-778-5613.
E-mail addresses: kawamiya@jamstec.go.jp (M. Kawamiya), aoschlies@ifm.uni-kiel.de (A. Oschlies).
[1] Fax: +49-431-600-1515.

0924-7963/02/$ - see front matter © 2002 Elsevier Science B.V. All rights reserved.
PII: S0924-7963(02)00241-5

To assess and improve our understanding of pelagic ecosystems, the extreme meteorological forcing in the Arabian Sea makes this region an ideal testbed. Numerical modeling forms an indispensable part of a project like JGOFS because it may enable us to fill the temporal and spatial gaps which inevitably exist in observational data, and thereby may allow us to infer causality in observed phenomena more strictly. It is also hoped that results from a numerical model will, in the future, help setting up observation plans by identifying the optimal temporal and spatial setting.

Zero or one-dimensional water column models, which are relatively economical in terms of computational cost, have frequently been used for ecosystem studies. Owing to their compactness, one can carry out many experiments, and therefore can adopt a trial-and-error approach to minimize discrepancies between model results and observations. Recently, this type of models has often been used for inversion studies, which can be considered as a mathematically formulated trial-and-error approach (e.g., Hurtt and Armstrong, 1996; Prunet et al., 1996a,b; Gunson et al., 1999; Schartau et al., 2001).

In contrast, three-dimensional models cost much more, but they can yield a more realistic physical environment for the embedded ecosystem model. Pioneering works using a model of this type on a basin scale were accomplished by Fasham et al. (1993) and Sarmiento et al. (1993). They illuminated the importance of the physical environment, showing that most of the differences in biological variables between the model results and observations could be ascribed to the model's failure in reproducing the appropriate physical structure in the upper ocean. Kawamiya et al., (2000a,b) also illustrated the importance of the physical environment using an ecosystem model for the Pacific Ocean; they demonstrated that the varying physical environment has the power to create the observed diversity in biological provinces described by Longhurst (1995).

A number of earlier three-dimensional coupled ecosystem-circulation modeling efforts have focussed on the Arabian Sea. Young and Kindle (1994) pointed out that the coastal upwelling and the subsequent horizontal advection are important for the silicate supply off the coast of Oman. Keen et al. (1997) obtained the related result that the horizontal advection is important for nitrate as well, and showed that the effect of horizontal advection is also reflected in the simulated chlorophyll distribution. Gallacher and Rochford (1995) studied the interannual variation of phytoplankton biomass using a proximate tracer for phytoplankton. It was shown that changes in the strength of wind stress and its curl can result in significant changes in phytoplankton biomass. They also pointed out that the satellite-measured interannual variation of chlorophyll reported by Brock and McClain (1992) may be an artifact caused by the timing of satellite measurements. In all of the above modeling studies, the reduced gravity (RG) model by Wallcraft (1991) was used for the physics. Using an RG model with 2.5 layers, McCreary et al. (1996) (referred to as MKHO) described the dynamics of the seasonal cycle in the Arabian Sea ecosystem. Based on the phytoplankton blooms simulated by their model, they proposed a classification into three types of blooms, namely, entrainment, detrainment, and upwelling bloom. Using basically the same model with the number of layers increased to 4.5, McCreary et al. (2001) discussed the importance of intraseasonal and diurnal variations in model forcing. The characteristics of seasonal variation in their model displayed high sensitivity to short-term variations in the atmospheric forcing. Ryabchenko et al. (1998) (referred to as RGF) performed a simulation with an ecosystem model coupled to a quasi geostrophic model forced by climatological data. Their results are in many aspects similar to those of MKHO, in spite of many differences in both the physical and the ecosystem model. Swathi et al. (2000) developed a coupled physical–biological–chemical model with a coarse resolution based on the GFDL primitive equation (PE) model, and obtained the result that the entire Arabian Sea is an outgassing region for CO_2, which is consistent with the global map of air–sea CO_2 exchange by Takahashi et al. (1999).

Recent development of computer architecture has made it feasible to run a PE model at higher, eddy-permitting resolution, as in the experiments for the Atlantic by Oschlies and Garçon (1998, 1999) and Oschlies et al. (2000). It is expected that this type of model provides a more realistic physical environment to an ecosystem model concerning, for example, nutrient injection to the surface due to eddies (Yoshimori and Kishi, 1994; McGillicuddy et al., 1998). Here we present results of such an ecosystem-circu-

lation model, which is a first application of a PE-based, eddy-permitting model to the Arabian Sea. The goal of our modeling exercise is to identify the points for which our current knowledge is sufficient or insufficient to explain dynamics of the Arabian Sea ecosystem, clarify the mechanism of simulated phenomena for which the model behaves realistically enough, and suggest some directions to which future efforts ought to be devoted. In this paper, as an essential first step to achieve the above goal, we compare the model results with observations in order to perceive the model's ability and inability to reproduce observed features. One can thereby obtain a sense of applicability of the model to more specific problems, e.g., the nitrate supply route during the southwestern monsoon (SWM) bloom (Kawamiya, 2001) or seasonal variations of the export ratio (Kawamiya and Kriest, submitted for publication), both of which require the perception of the model's ability to reproduce, among others, phytoplankton blooms and nitrate supply near the coast of Oman during SWM.

The model description is given in Section 2, followed by the comparison of the model results with observations for the physical fields in Section 3. The simulated biological fields are extensively compared with both climatological data sets and in situ measurements in Section 4. Section 5 puts our model results in perspective with earlier model studies and also discusses the results of sensitivity experiments. Summary and outlook are then provided in Section 6.

2. Model description

2.1. Physical model

The physical model is based on the Modular Ocean Model, version 2.1 distributed by the Geophysical Fluid Dynamics Laboratory (Pacanowski, 1995). It is a level model which solves the primitive equations. The settings specific to this study are exactly the same as used by Rix (1998). The model domain extends from 30°S to 26°N and from 30°E to 110°E, covering the entire Indian Ocean. The horizontal resolution is 1/3° both meridionally and zonally, permitting mesoscale eddies to exist in the model. Vertically it has 35 levels, 10 of which are situated in the upper 110 m (Table 1). Below this depth, level thickness increases gradually to 260 m at 5150 m. A realistic topography is incorporated in the model after regridding and smoothing the original data from ETOPO5.

Horizontal subgrid-scale mixing is resolved through a biharmonic operator with diffusion coefficients set to 2.5×10^{19} cm^4 s^{-1} for both mixing and dissipation. This formulation, proportional to the fourth partial derivative with respect to space, is highly scale-selective in that it applies stronger smoothing on smaller scales than on larger scales. This feature is desirable for an eddy-permitting model, where hori-

Table 1
Vertical levels of the model

Model level	Depth of grid point	Depth of grid box bottom	Thickness of grid box
1	5.00	10.00	10.00
2	15.00	20.00	10.00
3	25.00	30.00	10.00
4	35.00	40.00	10.00
5	45.00	50.00	10.00
6	55.00	60.00	10.00
7	65.00	70.00	10.00
8	75.00	80.00	10.00
9	85.00	91.85	11.85
10	98.69	110.95	19.10
11	123.20	144.07	33.12
12	165.94	197.02	52.95
13	229.10	274.25	77.23
14	319.40	378.56	104.31
15	437.73	510.92	132.36
16	584.10	670.35	159.43
17	756.60	854.07	183.72
18	951.54	1057.62	203.55
19	1163.69	1275.18	217.56
20	1386.67	1500.00	224.82
21	1613.34	1726.85	226.85
22	1840.37	1954.42	227.57
23	2068.47	2183.40	228.98
24	2298.32	2414.42	231.02
25	2530.51	2648.01	233.59
26	2765.51	2884.60	236.59
27	3003.69	3124.49	239.89
28	3245.28	3367.82	243.33
29	3490.36	3614.60	246.78
30	3738.84	3864.67	250.07
31	3990.51	4117.75	253.08
32	4244.99	4373.40	255.65
33	4501.81	4631.09	257.69
34	4760.37	4890.10	259.01
35	5020.00	5150.00	259.90

Units are in m.

zontal mixing on a scale larger than that of mesoscale eddies should be explicitly resolved as advection by eddies. In the vertical, we have adopted the parameterization by Pacanowski and Philander (1981) with the background diffusivity and viscosity set to 0.1 cm^2/s. This parameterization calculates diffusivity and viscosity through a Richardson number criterion and was originally developed for equatorial regions where vertical current shear is large.

At the southern and eastern boundary of the model domain, open boundary conditions by Stephens (1991) are applied. For the restoration of salinity and temperature, monthly mean data by Levitus and Boyer (1994a,b) are used with a restoring time scale of 25 days. For nitrate, annual mean data by Conkright et al. (1994a) are used. Restoration is necessary also for the other biological variables, which are simply damped to zero everywhere along the open boundaries. The barotropic part of the flow, which must be specified along the open boundaries, is taken from the global eddy-permitting model of Stammer et al. (1996) for the simulated year 1990, and its monthly mean is imposed along the boundaries.

The model is forced with climatological data sets. For the wind stress, monthly mean data compiled by Barnier et al. (1995) are used. Surface salinity is relaxed to the monthly mean values of Levitus and Boyer (1994a) with a damping time scale of 25 days. Heat flux at the sea surface is diagnosed by the method devised by Haney (1971). Data for heat fluxes and sea-level air temperature required for its implementation are taken from Barnier et al. (1995). Solar radiation is allowed to penetrate into the upper ocean, where the absorption occurs according to the formula by Paulson and Simpson (1977) for the water type I as defined by Jerlov (1968).

The advection scheme is based on central differentiation. A flux correction is applied for the variables of the ecosystem model to ensure positive values. This modified central differentiation was first introduced by Lafore et al. (1998) and is called multidimensional positive definite centered differences (MPDCD). A detailed description of MPDCD is also provided by Oschlies and Garçon (1999). This scheme has an advantage over upstream differentiation in that it bears much less computational diffusion for typical biogeochemical tracer distributions in the ocean (Oschlies and Garçon, 1999). However, the inherent problem with central differentiation, namely, overshooting, cannot be totally eliminated by the flux correction made by MPDCD.

2.2. Ecosystem model

The ecosystem model used here is almost the same as employed in a series of experiments for the North Atlantic by Oschlies and Garçon (1998, 1999) and Oschlies et al. (2000), with the difference being a lower value for the maximum grazing coefficient ($1\ day^{-1}$). In the North Atlantic experiments, a somewhat high rate ($2\ day^{-1}$) was assigned for grazing process to suppress an unrealistically strong spring bloom. This bloom is associated with a sudden shallowing of the mixed layer in the northern North Atlantic in spring when the simulated mixed layer depth (MLD) changes its value from >300 to <50 m within ~10 days. Such a large and rapid change of MLD does not take place in the Arabian Sea, leaving us no reason to maintain the high grazing pressure in the present model. Here we will only briefly summarize the model structure. A more complete description of the model is provided by Oschlies and Garçon (1999).

The ecosystem model consists of four compartments, that is, nitrate, phytoplankton, zooplankton, and detritus. These variables are expressed in terms of nitrogen concentration. Their time evolution is governed by the advection–diffusion equation with a source-minus-sink (sms) term, which describes the biological interactions:

$$\mathrm{sms}(P) = \overline{J}(z,t,N)P - G(P)Z - \mu_P P, \tag{1}$$

$$\mathrm{sms}(Z) = \gamma_1 G(P)Z - \gamma_2 Z - \mu_Z Z^2, \tag{2}$$

$$\mathrm{sms}(D) = (1-\gamma_1)G(P)Z + \mu_P P + \mu_Z Z^2 - \mu_D D - \frac{\partial(w_s D)}{\partial z}, \tag{3}$$

$$\mathrm{sms}(N) = \mu_D D + \gamma_2 Z - \overline{J}(z,t,N)P, \tag{4}$$

where P denotes phytoplankton, Z zooplankton, D detritus, and N nitrate; $\overline{J}$ is the daily averaged

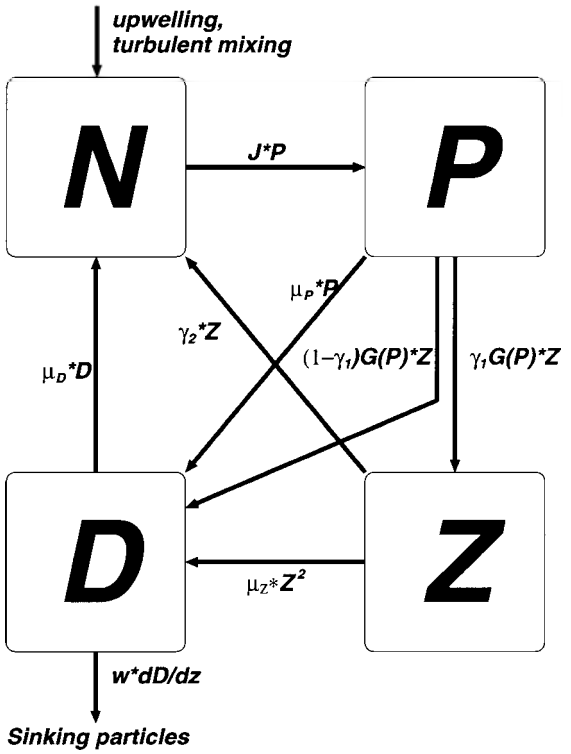

Fig. 1. Compartments and interactions of the biological model.

phytoplankton growth rate as a function of depth z and time t, and G is the grazing function. Fig. 1 gives a plain view of the interactions among the variables.

For the phytoplankton growth rate $\overline{J}$, we follow Hurtt and Armstrong (1996) who used the minimum of light- and nutrient-limited growth rate instead of the product among nutrient- and light-limitation factor and the maximum growth rate. The daily-mean light limited growth rate is calculated following Evans and Parslow (1985). The nutrient-limited growth rate is described by the Michaelis–Menten formula. The maximum growth rate increases with temperature according to Eppley (1972). For zooplankton grazing, we adopt a Holling type III function which gives a dependence of grazing rate on phytoplankton abundance with an S-like shape (cf., Fasham, 1995). The parameter values used in the standard experiment are listed in Table 2.

2.3. Integration

The physical model was spun-up by Rix (1998) with an integration of 25 years using the climatological wind stress. The spin-up was started from rest in January, with temperature and salinity taken from Levitus and Boyer (1994a,b). After the incorporation of the ecosystem model, the coupled model has been run for another 8 years (on-line integration). The initial nitrate concentration field was taken from Conkright et al. (1994b). For the initial concentrations of the other biological variables, values have been set to 0.1 mmolN/m^3 everywhere above 500-m depth,

Table 2
Parameters of the ecosystem model

Parameter	Symbol	Value	Units
Initial slope of P–I curve in the Evans and Parslow (1985) formulation	–	0.025	day^{-1} W^{-1} m^2
(Photosynthetically active radiation)/(Total irradiance)	–	0.43	–
Light attenuation due to water	–	0.04	m^{-1}
Light attenuation by phytoplankton	–	0.03	m^2 mmol^{-1}
Maximum growth rate parameters in the Eppley (1972) formulation ab^{cT} (T: temperature in Celsius)	a	0.6	day^{-1}
	b	1.066	–
	c	1.0	°C^{-1}
Half-saturation constant for N uptake in the Michaelis–Menten formula	–	0.5	mmol/m^3
Specific mortality rate of phytoplankton	μ_P	0.03	day^{-1}
Assimilation efficiency	γ_1	0.75	day^{-1}
Maximum grazing rate in the Holling type III function	–	1.0	day^{-1}
Prey capture rate in the Holling type III function	–	1.0	day^{-1} mmol^{-2} m^6
Quadratic morality of zooplankton	μ_Z	0.20	day^{-1} mmol m^3
Excretion rate of zooplankton	γ_2	0.03	day^{-1}
Remineralization rate of detritus	μ_D	0.05	day^{-1}
Sinking velocity of detritus	w_s	5.0	m/day

and zero below. Results are presented for the average over the third to eighth year of the coupled integration unless otherwise specified.

In the third year of integration, the ecosystem model already establishes the stationary cycle except for nitrate which still has a long-term trend in the subsurface depths of ~100–300 m. This can be partly accounted for, as will be shown later, by the neglect of denitrification in the model. Regarding this trend, physical processes with a long time scale such as vertical diffusion of nitrate are also important, and reaching the complete equilibrium state would require an integration period of several hundred years, which is not feasible at eddy-permitting resolution. However, since the initial nitrate field is taken from a climatology, the first few years of integration should give a realistic estimate of the amount of nitrogen available for the surface ecosystem. We believe that it is meaningful and, because of the neglect of denitrification, even preferable to analyze the model results before the model reaches complete equilibrium.

3. Physical fields

3.1. Salinity, temperature, and density

Simulated and observed annual mean distributions of salinity, temperature, and density are depicted in Fig. 2 along 65°E for the upper 300 m in order to see whether the model properly reproduces the water mass structure in the Arabian Sea as described by Shetye et al. (1994), Morrison et al. (1998), and references therein. The model captures the southward penetration of a water mass with high salinity at the depth of ~80 m. This high salinity water in the model may correspond to Arabian Sea Water, which is produced by evaporation and cooling caused by the northeast monsoon (NEM). At greater depths, however, the model fails to reproduce the high salinities north of 10°N. A possible reason is that the model lacks the formation of Red Sea Water (RSW) and Persian Gulf Water (PGW), both of which have high salinity (~35.5 and 36.0 psu, respectively). Because the core of RSW is on a relatively deep isosurface (27.2 σ_ϑ), its absence in the model has probably less impact on upper ocean biology than that of PGW, which is centered at 26.6 σ_ϑ.

Temperature at depths greater than 200 m in the model is higher than the observed north of 10°N. This may again be caused by the absence of PGW. Because the discrepancy in temperature is compensating that in salinity in terms of density anomaly, the vertical section for density is quite similar between the model and the observation. The pycnocline is, however, sharper in the model which might be due to overly strong smoothing in the climatological data. Although no explicit smoothing has been applied vertically to create the climatology, time averaging may loosen the vertical gradient in a density profile with a sharp pycnocline whose depth changes every year. The problem would be less serious for the 6-year mean model results, since the model is driven by the same forcing data every year and the differences in pycnocline depth over years would be much smaller than in reality.

3.2. Mixed layer depth

MLD influences light conditions for phytoplankton and its accurate representation is thus very important for the ecosystem model. Fig. 3 shows the MLD computed from the model and from climatological data for January and August, corresponding to the maximum phase of the NEM and the SWM, respectively. The observational fields for the MLD are derived from climatological data sets for temperature (Antonov et al., 1998) and salinity (Boyer et al., 1998). Here, MLD is defined as the depth in the water column at which the density difference with respect to the sea surface first exceeds the critical value corresponding to temperature difference of 0.5 °C. In January, it is well reproduced that MLD is large in the northwestern part, though mixed layers are deeper by some 10–20 m in the model. In August, the model results again resemble the observation in that the ML is deepest in the central Arabian Sea and is moderately deep near the coast of Somalia; the maximum values of ~100 m also agree well with observations, although the exact location of the maximum is shifted to the south in the model compared with the observation.

As Oschlies et al. (2000) pointed out, calculating MLD from climatological temperature and salinity data may underestimate maximum values because of the smoothing out of extreme events arising from, for

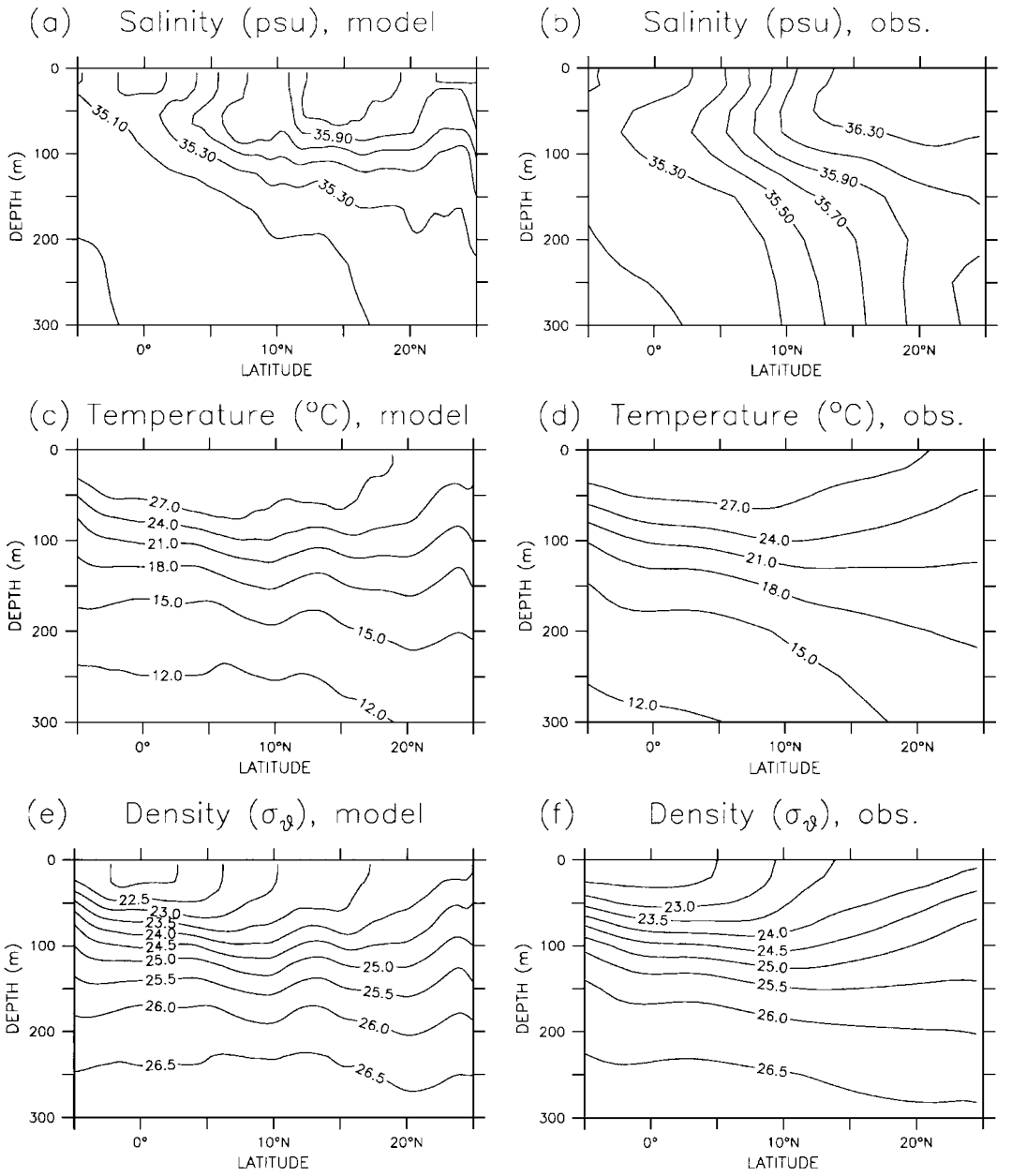

Fig. 2. Annual mean fields along a vertical section at 65°E for (a) simulated and (b) observed salinity, (c) simulated and (d) observed temperature, and (e) simulated and (f) observed density. The data are taken from Antonov et al. (1998) and Boyer et al. (1998). Units are indicated in each panel.

example, interannual variability in the time of deepest mixing. Rao et al. (1989) created a climatology of MLD for the Indian Ocean based on values derived from each individual profile. Their map, which should be free from this smoothing error, shows values similar to those in Fig. 3c for February, and higher by ~ 20 m than in Fig. 3d for August. Unfortunately, this does not remove the problem of the model's

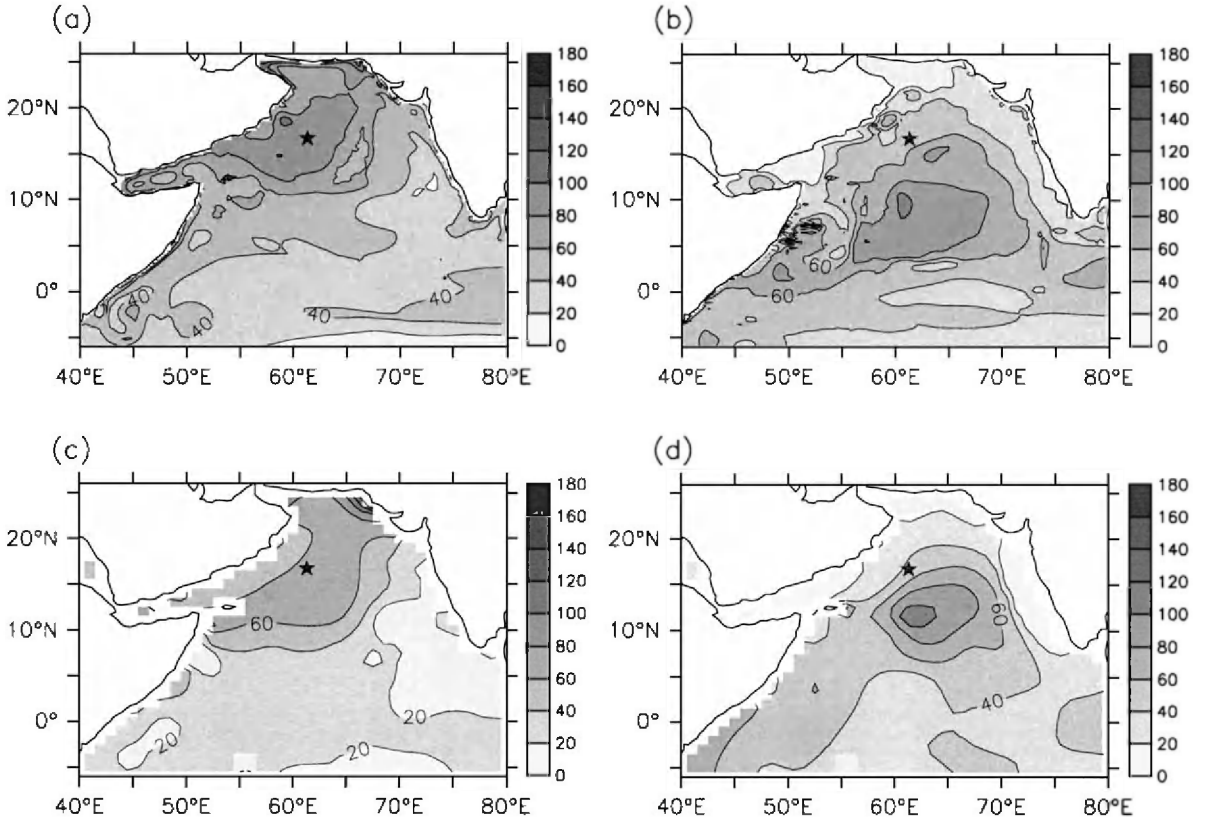

Fig. 3. Mixed layer depth for (a) the model averaged for January and (b) August, and (c) observations in January and (d) August. The observational fields are derived from the data of Antonov et al. (1998) and Boyer et al. (1998). Units are in m. The location of the WHOI mooring site (15.5°N, 61.5°E) is indicated by a star.

overestimate of MLD in February and even adds a new one of a possible underestimate in August. The data for MLD from the WHOI mooring site (15.5°N, 61.5°E, indicated by a star in Fig. 3) exhibit values of 80–100 m in January and 30–40 m in August (Dickey et al., 1998). They agree well with the model in January but are deeper by 20 m in August, which is consistent with the above comparison between the model result and the data by Rao et al. (1989).

4. Biological fields

4.1. Basin-wide comparison

4.1.1. Nitrate

Fig. 4 shows the annual mean nitrate distribution averaged over the upper 150 m. The model reproduces the main features seen in the observations (Conkright et al., 1998): nitrate concentrations are extremely high (>15 mmol/m^3) along the coast of Oman, moderately high (~ 10 mmol/m^3) near the tip of Somalia and along the western coast of India, and they are lowest (~ 6 mmol/m^3) in the central Arabian Sea. The upwelling along the coasts during SWM seems to be the main cause for the high abundance of nitrate in the western Arabian Sea.

Conspicuous differences between the two figures include the following: the simulated nitrate concentration is higher in the northern end of the domain; the width of the area with high concentration along the coast of Oman is much narrower in the model; and the isolated maximum in the observation around Seychelle Bank (~ 5°S, 55°E) is not found in the simulation. Because the spatial extent of the Arabian Sea is not large, these differences can at least

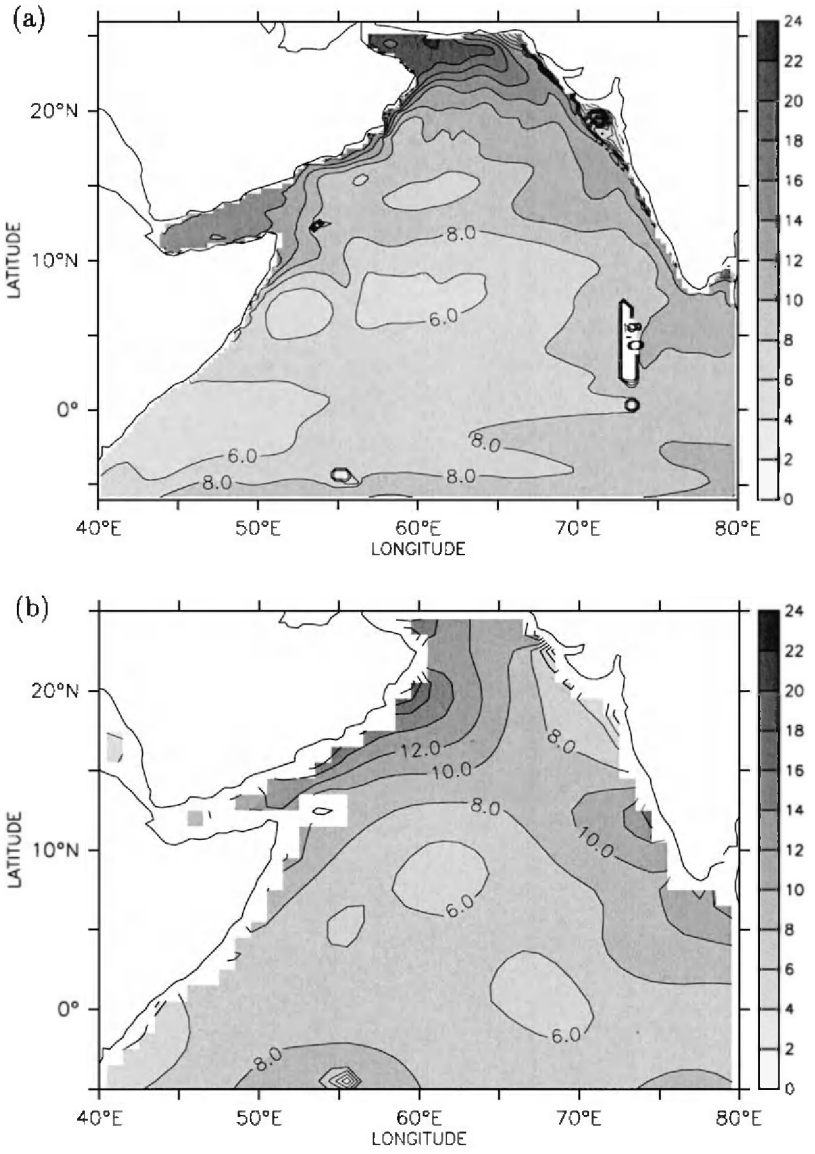

Fig. 4. Annual mean nitrate distribution averaged over the upper 150 m for (a) the model simulation and (b) the data of Conkright et al. (1998). Contour intervals are 2 mmol/m^3.

partly be attributed to the strong smoothing in the data of Conkright et al. (1998). Concerning the discrepancy near Seychelle Bank, the peculiar nitrate distribution on a vertical section crossing Seychelle Bank (figure not shown) suggests that the rough topography around there may have an effect to increase surface nitrate through, for example, tidal mixing, which is not accounted for in the present model. The overestimation in the northern end is most evident in the Oct.–Dec. season (figure not shown), and is definitely related to the overestimated nitrate maximum in subsurface waters which is seen in Fig. 5, where annual mean nitrate along 65°E is depicted.

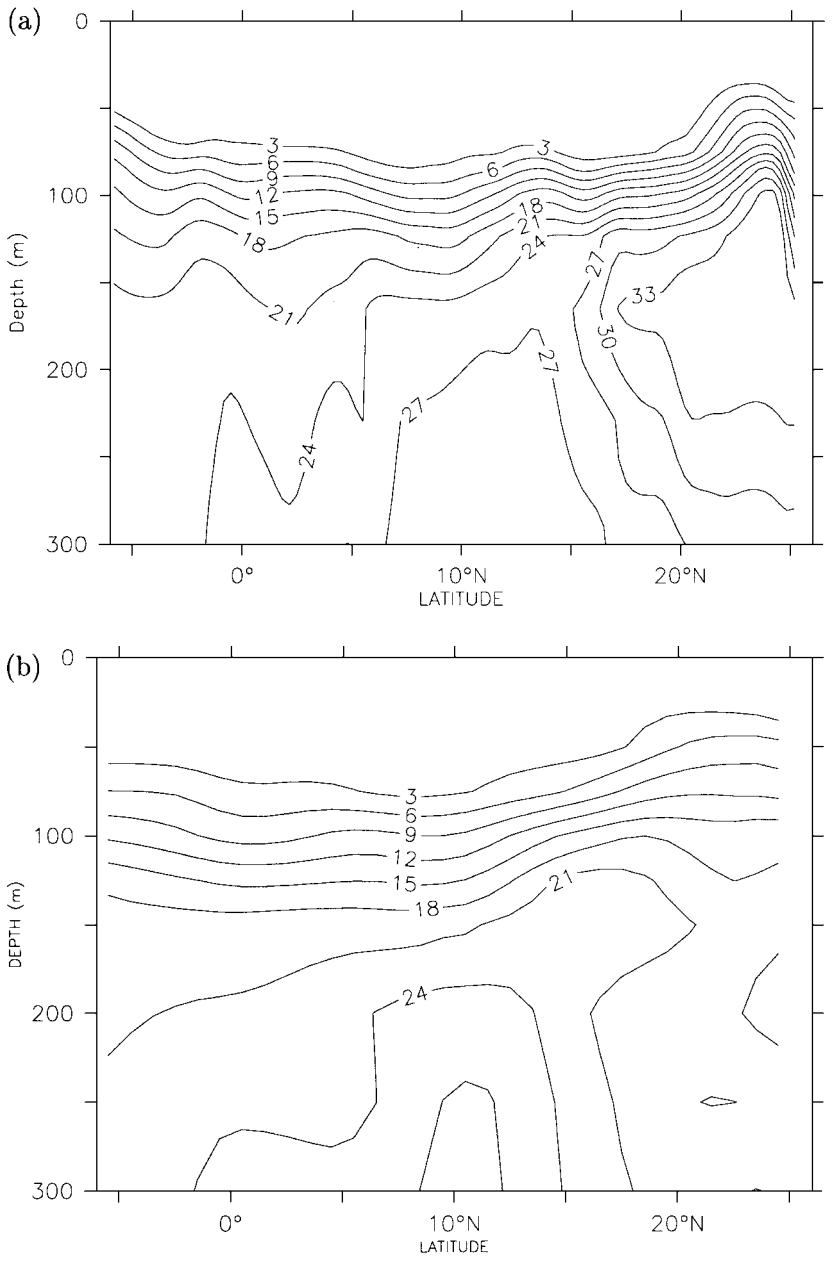

Fig. 5. Annual mean nitrate distribution along a vertical section at 65°E for (a) the model simulation and (b) the data of Conkright et al. (1998). Contour intervals are 3 mmol/m^3.

The simulated distinct nitrate maximum shown in Fig. 5 centered at ~ 150 m, north of 20°N is not found in the observations. Instead, there is even a nitrate minimum below the depth of the simulated maximum. The observed minimum is known to be caused by denitrification (e.g., Naqvi, 1994), a process which is presently not incorporated in the model. Because denitrification can take place only when

Table 3
Estimates of the denitrification rate for the Arabian Sea

Study	Rate (TgN/year)	Method
Naqvi (1987)	29.5	Box model
Mantoura et al. (1993)	11.9 ± 5	Nitrate deficit + residence time
Naqvi and Shailaja (1993)	24–33	ETS (direct measurement)
Howell et al. (1997)	21 ± 7	Nitrate deficit + CFC age
Yakushev and Neretin (1997)	34.1	One-dimensional model
Bange et al. (2000)	6–60	Nitrate deficit + residence time
This study	11–24	Trend in nitrate increase

dissolved oxygen is depleted, the occurrence of this process often coincides with abundant organic matter. Without the denitrification process, simulated nitrate will continue to increase through remineralization when the ambient water is extremely rich in detritus. In reality, on the other hand, nitrate would not be allowed to increase in this region and would even decrease by denitrification. This may be one reason why the simulation reveals a nitrate maximum near the place where a minimum is found in the observations.

The amount of nitrate integrated over the Arabian Sea to the north of 10°N and down to 670 m increases steadily by ~ 16 TgN/year over the third to eighth year of integration. This trend should give an approximate estimate of denitrification over the northern Arabian Sea, if the loss of nitrate through denitrification is largely in balance with advective input of nitrate in reality (Bange et al., 2000). One may argue that this number may be biased to the

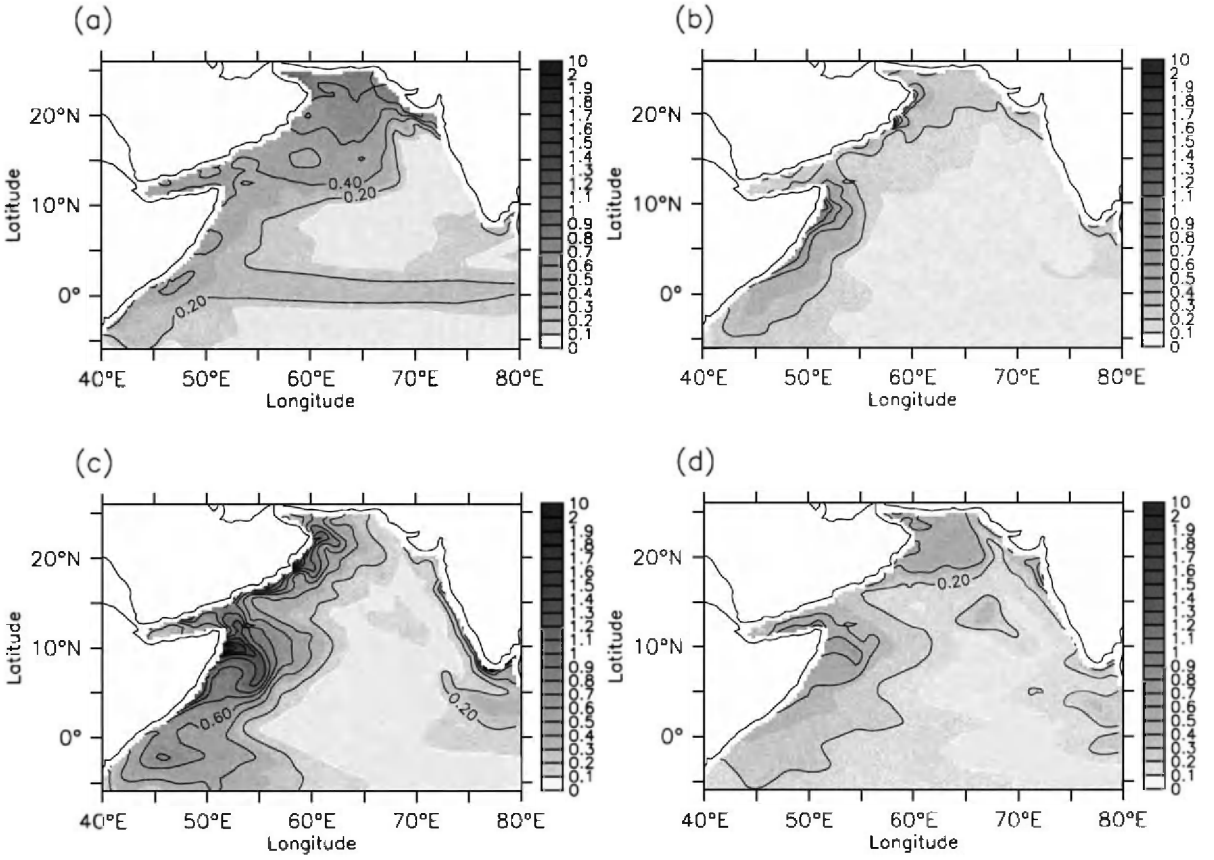

Fig. 6. Simulated chlorophyll distribution averaged over the period (a) Jan.–Mar., (b) Apr.–Jun., (c) Jul.–Sep., and (d) Oct.–Dec. Averaging has been also applied over the upper 0–20 m. Contour intervals are 0.2 mg/m^3 for contour lines and 0.1 mg/m^3 for shades.

larger side because of the relatively slow sinking velocity of detritus in the model (5 m/day) and the consequential remineralization that is almost completed within the upper few hundred meters. There is, however, a significant increasing trend of subsurface nitrate (11 TgN/year) also in a sensitivity experiment with a much faster sinking (10 m/day in the upper 144 m, instantaneous sedimentation following the Martin et al. (1987) curve below), as will be shown in Section 5.2. For a number of sensitivity experiments, the rate varies within the range of 11–24 TgN/year (Section 5.2). The values are within the range of past estimates of the integrated denitrification rate in the northern Arabian Sea (Table 3). An effort to explicitly incorporate the denitrification process in the present model is underway. Denitrification in the northern end of the Arabian Sea, and the formation process of the corresponding nitrate minimum, have been the subject of many earlier studies (Naqvi, 1994; Morrison et al., 1999, and references therein).

Another contribution to the model's too high nitrate concentrations in this region may arise from the above-mentioned lack of PGW production in the model. This water mass is known to have lower nitrate concentration and lies at the isosurface of 26.6 σ_θ. To obtain an idea on the extent to which PGW dilutes concentrations in the nitrate maximum region, we have conducted an experiment in which the production of PGW is emulated using restoration

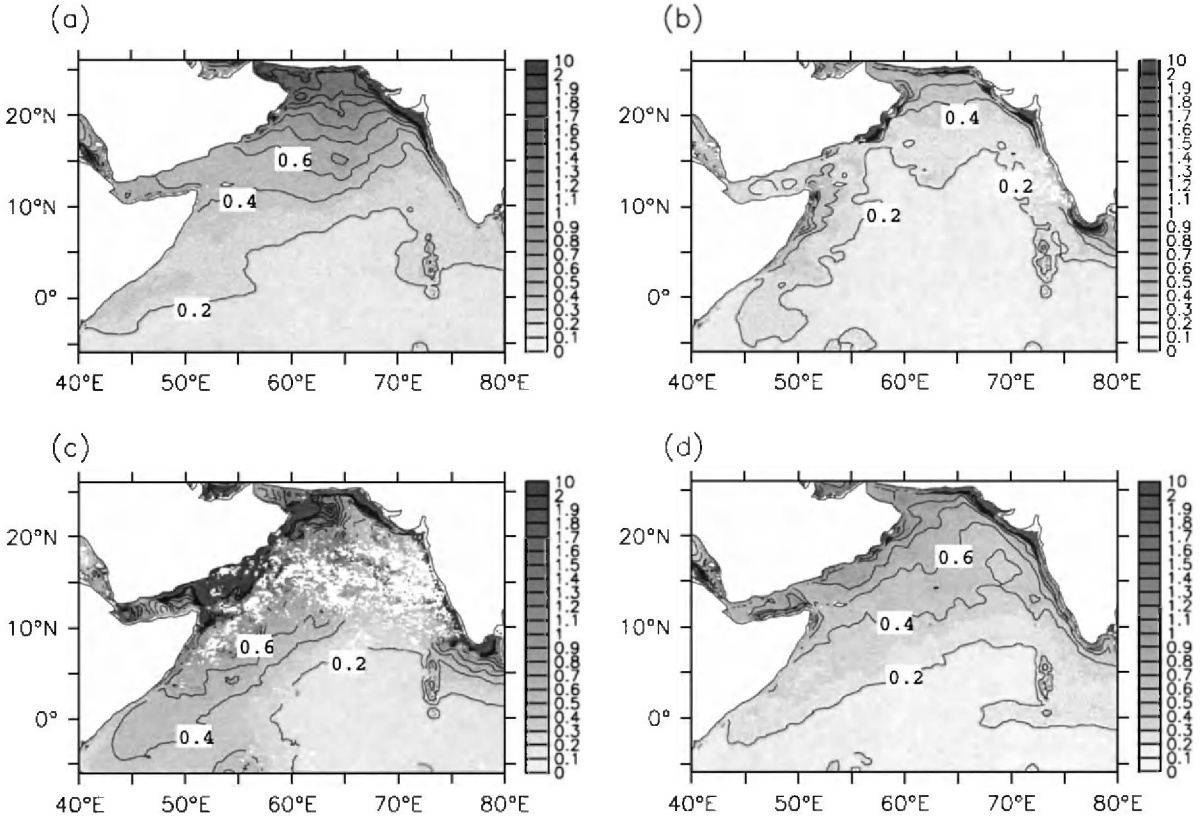

Fig. 7. Chlorophyll distribution based on SeaWiFS measurements during Oct. 1997–Sep. 2000, averaged over the period (a) Jan.–Mar., (b) Apr.–Jun., (c) Jul.–Sep., and (d) Oct.–Dec. Contour intervals are 0.2 mg/m^3 for contour lines and 0.1 mg/m^3 for shades. SeaWiFS data are provided by the Earth Observing System Data and Information System (EOSDIS), Distributed Active Archive Center at Goddard Space Flight Center which archives, manages, and distributes this data set through funding from Earth Observing System of NASA's Mission to Planet Earth.

toward observations in the area to the north of 24° and the west of 60°E. The resultant reduction in nitrate concentrations is, however, not more than ~ 2 mmol/m^3 (figure not shown). It seems therefore unlikely that the lack of PGW production is the main cause for the unrealistic nitrate maximum in our model.

While this discrepancy in the northern part of the Arabian Sea is obviously an issue that will need to be fixed, it should be noted that other features, like the depth at which nitrate begins to increase and its northward shoaling, are reproduced well in the model. For example, the depth of the contour line for 3 mmol/m^3 is ~ 70 m at 10°N in both the model and the climatology, and it shoals up to ~ 40 m to the north of 20°N. Besides, the nitracline is slightly steeper in the model. This may be again due to the smoothing applied when creating the climatology.

4.1.2. Chlorophyll

The seasonal variation of surface chlorophyll obtained from the model is displayed in Fig. 6. Chlorophyll values are calculated by multiplying the nitrogen-based concentration of the modeled phytoplankton by a factor of 1.59 gChl/molN, which corresponds to a chlorophyll to carbon mass ratio of 1:50 and a C/N mole ratio of 106/16. This conversion factor will be used throughout this paper. For comparison, SeaWiFS satellite measurements for the period Oct. 1997–Sep. 2000, and in situ data compiled by Conkright et al. (1998) based on long-term historical in situ data, are shown in Figs. 7 and 8, respectively. The main temporal and spatial patterns

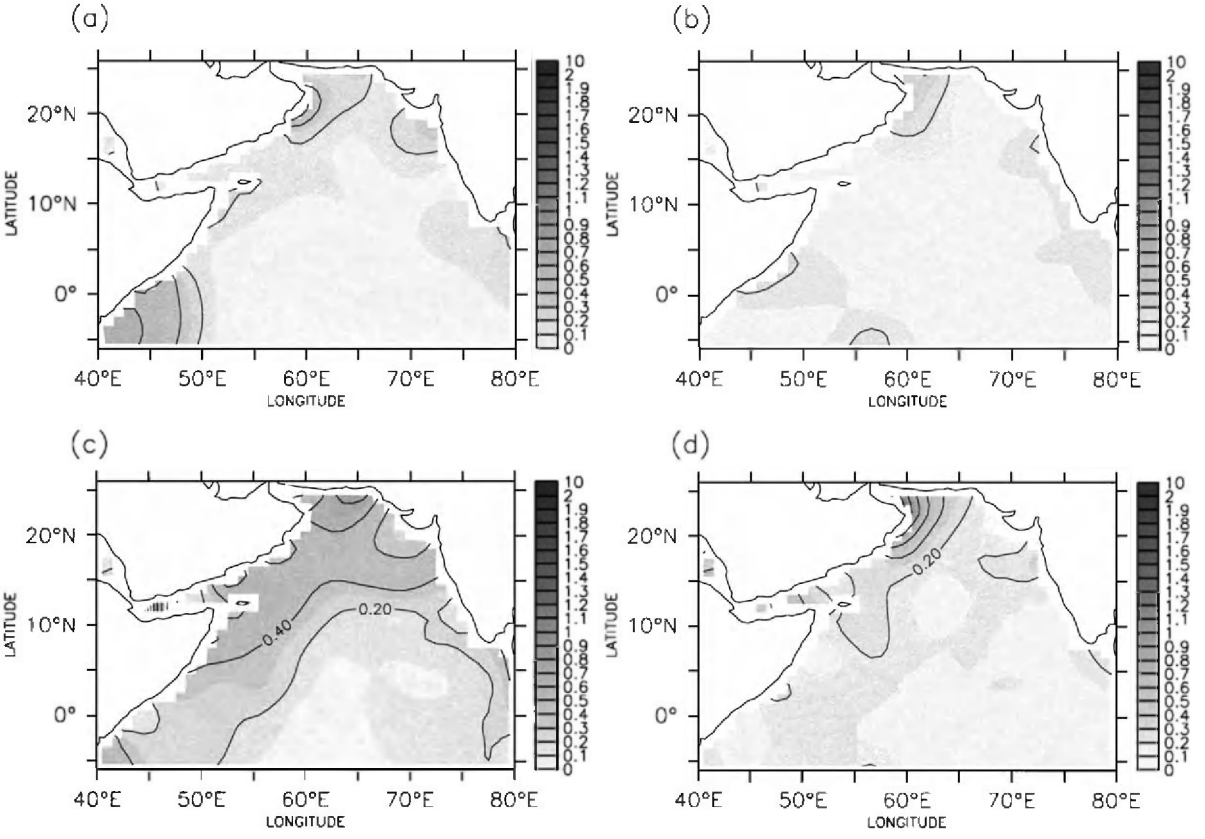

Fig. 8. Surface chlorophyll distribution from the data of Conkright et al. (1998) for the period (a) Jan.–Mar., (b) Apr.–Jun., (c) Jul.–Sep., and (d) Oct.–Dec. Contour intervals are 0.2 mg/m^3 for contour lines and 0.1 mg/m^3 for shades.

of the surface chlorophyll distribution are well reproduced by the model: chlorophyll concentration is high in summer (Jul.–Sep.) in the northwestern region of the domain and is quite low in spring (Apr.–Jun.) throughout the basin except for some coastal regions. Values are generally high in coastal regions and low in the central Arabian Sea.

For a more quantitative perspective, significant differences can be found between the different observations. Firstly, chlorophyll is much more abundant in regions very close to the land throughout the year in the SeaWiFS data. Large errors in the satellite measurements near coasts and the strong smoothing by Conkright et al. (1998) may be the cause(s) for the difference. We will not pay too much attention to this issue because the model does not include processes such as tidal mixing or nutrient supply from the land that can enhance biological activity in coastal regions.

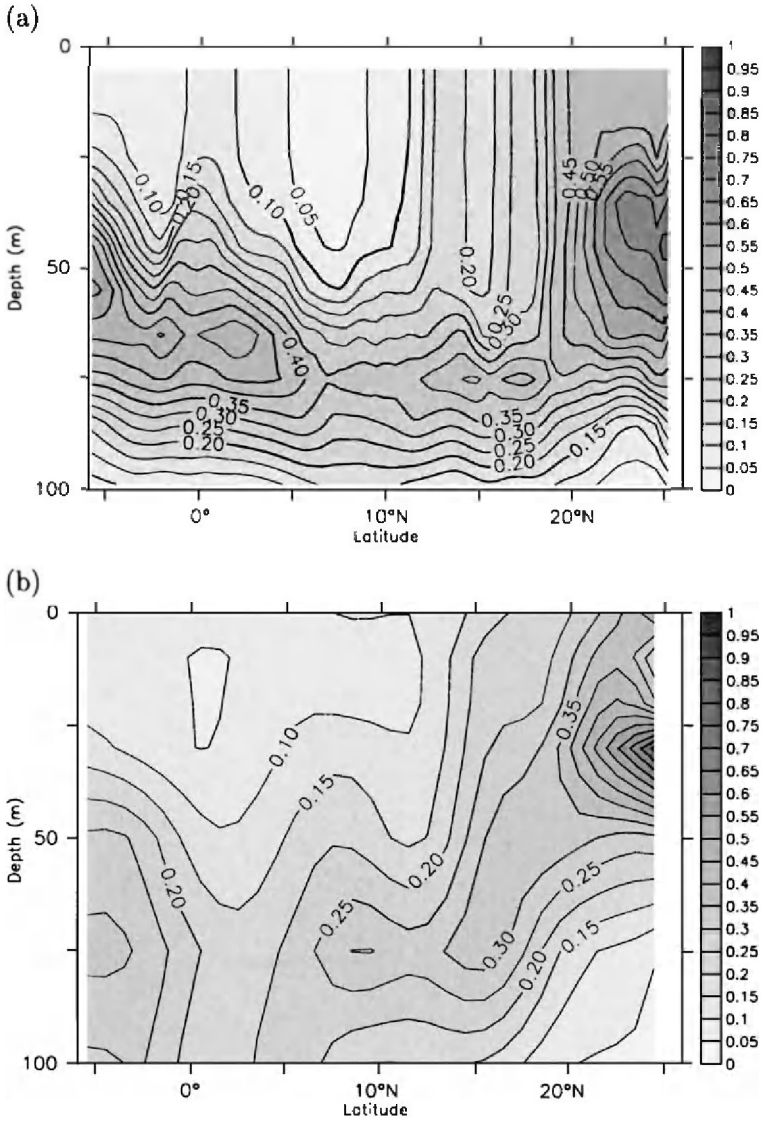

Fig. 9. Annual mean chlorophyll distribution along a vertical section at 65°E for (a) the model simulation and (b) the data of Conkright et al. (1998). Contour intervals are 0.05 mg/m^3.

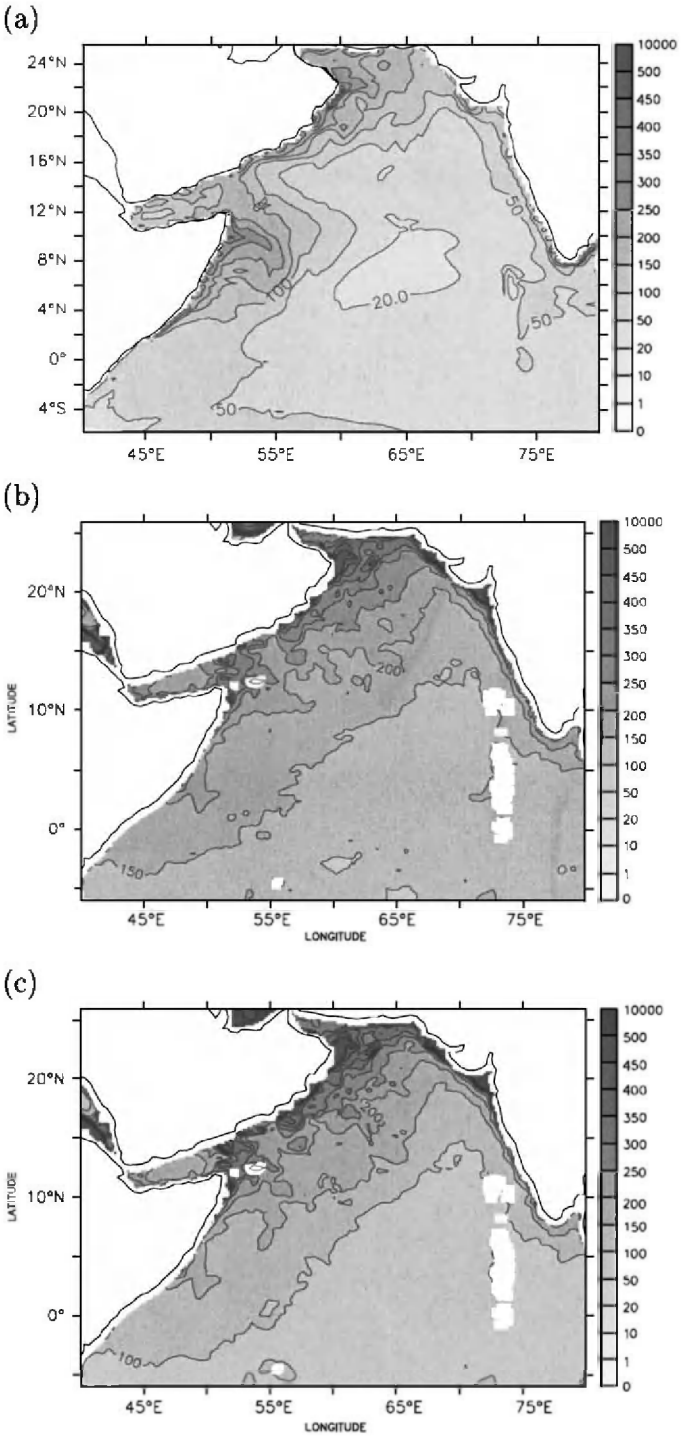

Fig. 10. Distribution of annual primary production for (a) the model simulation, (b) the data of Antoine et al. (1996) (available from http://www.obs-vlfr.fr/jgofs2/modelisation/globe.htm), and (c) those of Behrenfeld and Falkowski (1997) (http://www.marine.rutgers.edu/opp/). Units are in gC m^{-2} $year^{-1}$.

Secondly, during summer, phytoplankton blooms are far more intense in the SeaWiFS data than in the data of Conkright et al. (1998) (Figs. 7c and 8c). In the former, the concentration can reach up to ~ 4 mg/m^3 while it is at most ~ 0.5 mg/m^3 in the latter. While it is again possible that the smoothing by Conkright et al. (1998) obscured the blooms, one should also be aware of the fact that the extreme summer coastal blooms have not been directly confirmed yet by in situ observations. Latasa and Bidigare (1998), for example, found chlorophyll concentrations observed during SWM much lower than expected from SeaWiFS measurements. Though it may be the case that all the observations carried out so far have missed the blooms, it is also possible that chlorophyll concentrations during SWM have been overestimated by SeaWiFS. Indeed, the satellite measurements can be erroneous in this season because of almost constant cloud cover and high sea salt aerosol concentrations (Tindale and Pease, 1999). The model simulates chlorophyll moderate values between those measured by SeaWiFS and reported by Conkright et al. (1998).

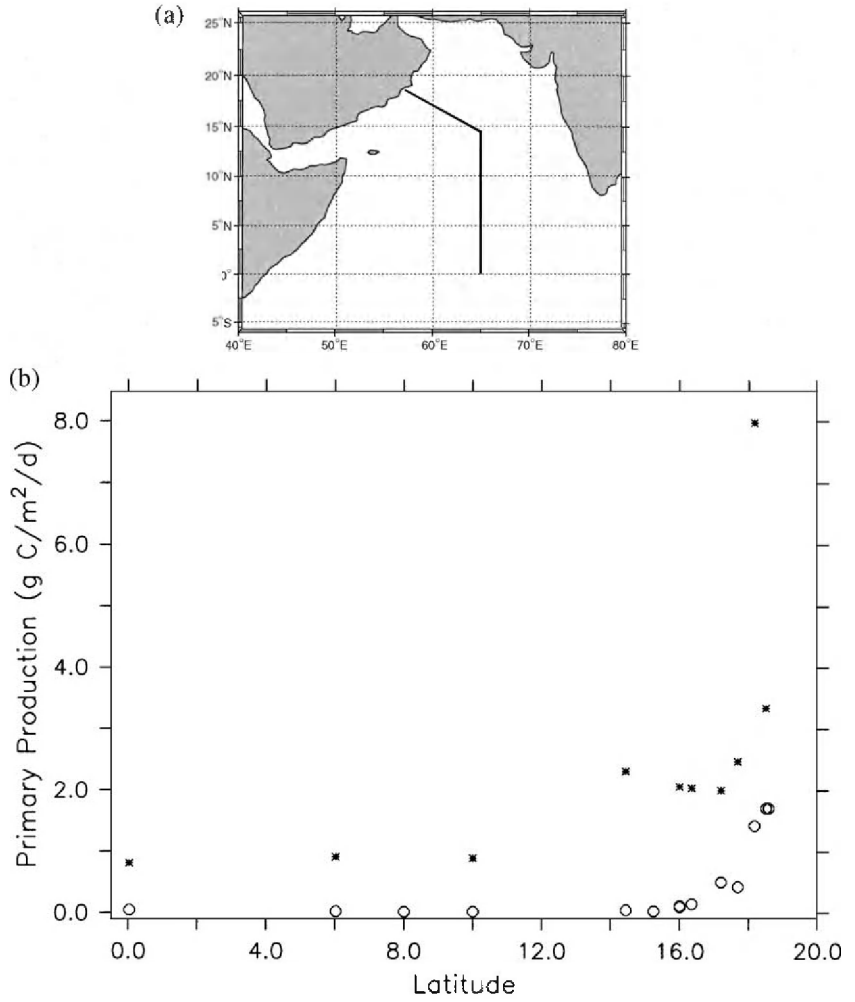

Fig. 11. (a) Observation line of the German JGOFS R/V METEOR's cruise M32/5 during Jul. 18–Aug. 11, 1995. (b) Vertically integrated primary production observed during the cruise (asterisks, data courtesy of Klaus v. Bröckel at IfM Kiel) and retrieved correspondingly from the model result (circles).

A model-data comparison for the annual mean vertical chlorophyll distribution is shown in Fig. 9. It is seen that the model reproduces the depth of the deep chlorophyll maximum (DCM), though the simulated concentrations are larger by ~ 40%. In both the model and the observations, the depth of DCM becomes shallow toward the north and follows the latitudinal variation of the nitracline (Fig. 5). As a result, the chlorophyll concentration at the DCM is highest at the northern end. The model fails, however, to simulate the very low concentrations at the equator which is seen in the observations throughout the water column. This model-data misfit can be related partly to the modest chlorophyll maximum in the model along the equator in northern winter (Jan.–Mar.), which is caused by equatorial upwelling exerted by the westward component of wind stress. While it should be kept in mind that the number of observations near the equator is quite small especially in northern winter, some overestimation of chlorophyll concentration along the equator is a typical problem of current basin-scale ecosystem models (e.g., Fasham et al., 1993; Oschlies and Garçon, 1999; Kawamiya et al., 2000a), the cause of which has not been clearly identified so far.

4.1.3. Primary production

Various estimates of primary production on a global scale are available based on CZCS satellite data, e.g., those by Longhurst et al. (1995), Antoine et al. (1996), and Behrenfeld and Falkowski (1997). Results from the latter two groups are shown in Fig. 10b and c. In Fig. 10a, the simulated annual primary production is displayed.

Note that there are considerable differences even between Fig. 10b and c, although both estimates are based on the same satellite data. Behrenfeld and Falkowski (1997) found a tendency that the estimate by Antoine et al. (1996) is larger in oligotrophic regimes with low primary productivity than that observed by them and vice versa. Behrenfeld and Falkowski (1997) ascribed this mainly to the different consideration of temperature effects in the respective primary production models. Satellite-derived estimates by Longhurst et al. (1995) show higher values throughout the Arabian Sea than the other two data sets. In

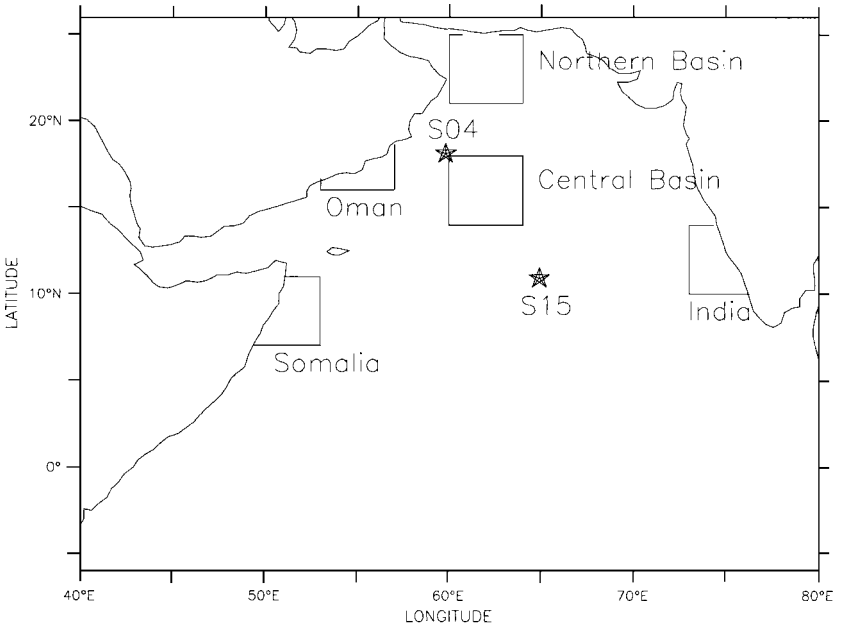

Fig. 12. Locations of the two selected stations of the U.S.JGOFS Arabian Sea Process Study, S04 and S15 (stars). Also shown are the areas over which averages have been computed for Fig. 18.

spite of these variations in satellite-based estimates, the model constantly yields lower primary production, both in regions with high (northwestern part and west coast of India) and low (the rest) annual primary production. The underestimate in the northwestern part may be attributed to the possible overestimate of chlorophyll by ocean color measurements mentioned before. This can, however, not account for the model's too low values in the central Arabian Sea. Indeed, a comparison of the model results for the SWM period with in situ data, e.g., those observed during a German JGOFS cruise (Fig. 11), reveals that the model gives relatively good estimates near the coast of the Oman while simulated primary production is too low in the central Arabian Sea.

Oschlies et al. (2000), in their model of the North Atlantic, identified a similar problem of too low primary production in oligotrophic regimes. The problem was even more serious in their case because their simulated primary production in oligotrophic regions was almost two orders of magnitude lower, while it is "only" by several times lower in the present case. This difference is caused by the fact that the nitracline is located at much shallower depths in the Arabian Sea than in the subtropical North Atlantic. Hence, modeled phytoplankton in oligotrophic regimes in the Arabian Sea can find more nitrate near the bottom of the euphotic zone than in the Atlantic. To improve simulated levels of primary production in oligotrophic regimes, Oschlies et al. (2000) suggested to include a loop for very fast recycling of nitrate within the euphotic layer. An experiment with this modification showed dramatically improved agreement between the model and the satellite-based observations (Oschlies, 2001). Results from the experiment in which this modification is applied to the present model will be shown in Section 5.2.1.

Although a high recycling rate in oligotrophic environments helps to increase primary production, it is of course possible that other processes are responsible for the model's underestimation. For example, Kriest (2000) proposed the production of dissolved organic matters (DOM) with high C/N ratios as a possible reason for the apparent discrepancy between carbon-based primary production measurements and nitrogen-based model results; a part of the DOM production could be detected by the common ^{14}C method (Karl et al., 1998), and the resultant carbon-based primary production could take on values much higher than those converted from a nitrogen-based estimate by the Redfield ratio. Kriest (2000) further made a first attempt to include such production in her model and obtained a better fit for carbon-based production between the model and the observations in oligotrophic situations. The results suggest, however, that the fast recycling of nitrate is still required though to a lesser extent.

If the production of DOM with high C/N ratios accounts for the discrepancy between high values of measured carbon-based primary production and lower simulated nitrogen-based primary production, the simulated nitrogen-based export ratio should be approximately the same as observed nitrogen-based *f*-ratios (the ratio of nitrate-based primary production to total nitrogen-based primary production). Available data do not support this DOM hypothesis; McCarthy et al. (1999) report that *f*-ratios during NEM are ~ 0.15, while the simulated export ratio across 110-m depth, averaged over NEM and the Arabian Sea, is 0.38. This disagreement does not exclude the possibility that the DOM production with high C/N ratios is occurring in other seasons. In addition, nitrogen fixation, which may contribute to the total primary production particularly in oligotrophic regimes during intermonsoon seasons, is not accounted for by the present model configuration.

The simulated annual primary production integrated over the domain shown in Fig. 10 is 0.716 PgC (70.1 gC/m^2). As expected, this is significantly lower than

Fig. 13. Model results averaged over the area 16.7–17.7°N, 59.3–60.3°E for (a) nitrate, (b) chlorophyll, and (c) detritus flux at 110-m depth (solid line). This area corresponds to the station S04 in U.S.JGOFS Arabian Sea Process Study. Dashed lines in (c) show the range of the standard deviation within the area. Units for (a) and (b) are in $mmol/m^3$. In (c), crosses denote observations of nitrogen flux taken at 800-m depth, which have been converted to that at 110 m using the empirical equation by Martin et al. (1987). The nitrogen flux data are available at http://www1.whoi.edu/arabian.html by courtesy of Susumu Honjo. Asterisks are the data by Buesseler et al. (1998) for the sinking flux across 100 m derived from ^{234}Th measurements. The horizontal error bars denote the durations of cruises corresponding to the respective flux data, which are also similar to the underlying time scale of the ^{234}Th method, i.e., the half value period of ^{234}Th (24.1 days).

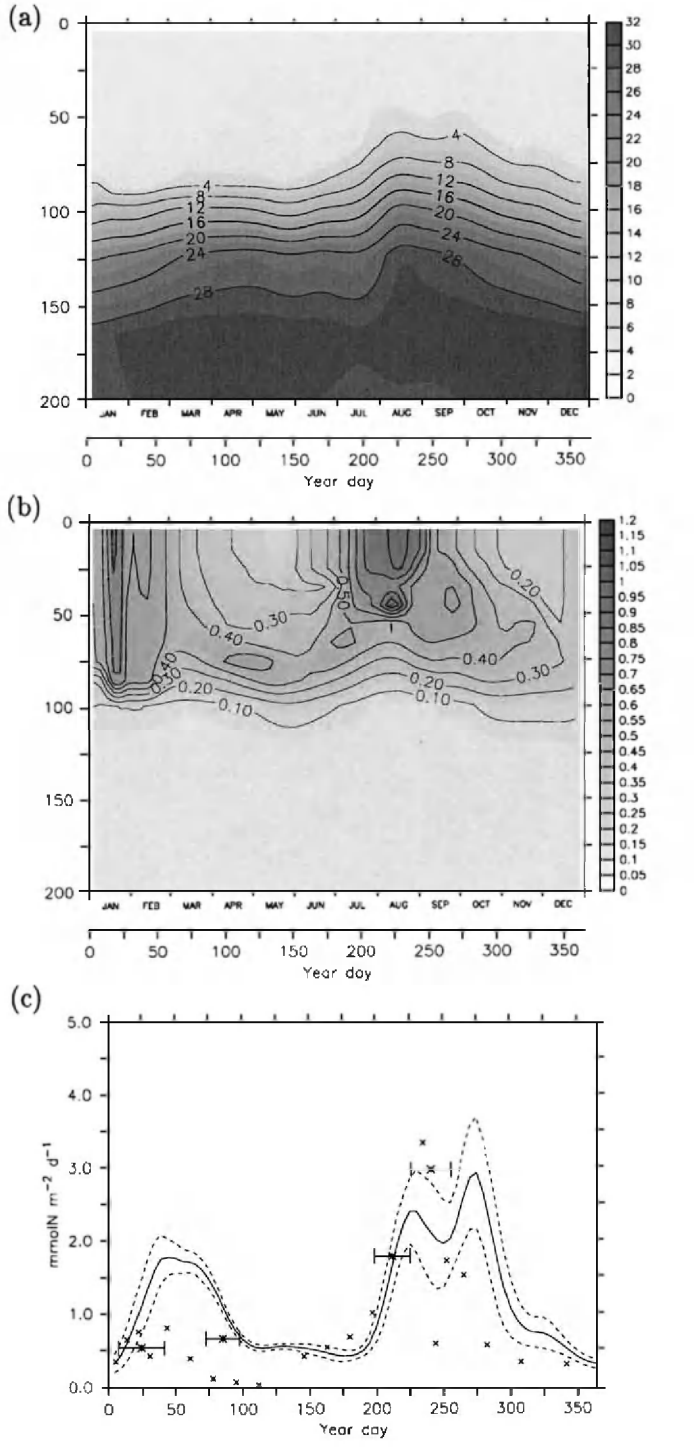
(a)
(b)
(c)
Year day
mmolN m^{-2} d^{-1}
JAN FEB MAR APR MAY JUN JUL AUG SEP OCT NOV DEC

the values that correspond to the estimates by Behrenfeld and Falkowski (1997) and Antoine et al. (1996), namely, 1.55 PgC (153 gC/m^2) and 1.87 PgC (184 gC/m^2), respectively. The simulated detritus flux exported across 110-m depth is 0.276 PgC (27.6 gC/m^2) when integrated over the area. Watts et al. (1999) estimated new production by multiplying satellite-based primary production by an *f*-ratio measured in situ. The obtained annual new production is ~ 0.5 PgC for an area similar to that shown in Fig. 10, and is twice as large as the detritus export in the model. Their average *f*-ratio of 0.3 is similar to the simulated export ratio calculated at 110-m depth (0.39). Considerably lower *f*-ratios were obtained by McCarthy et al. (1999) (~ 0.15 for NEM), and the carbon-based export ratios by Lee et al. (1998) and Buesseler et al. (1998) are even lower (~ 0.25 for SWM, ~ 0.05 for other seasons). Possible reasons why *f*-ratios may take on higher values than export ratios include nitrification near the bottom of the euphotic zone reported by Ward et al. (1989), who investigated the pathways of nitrogen transformations following the nitrogen isotope ratio in surface and subsurface waters in the Southern California Bight. The DOM production with high C/N ratios mentioned earlier may also result in nitrogen-based *f*-ratios being higher than carbon-based export ratios.

4.2. Comparison at JGOFS stations

Here we present comparisons between the model results and observations at two stations of the U.S.JGOFS Arabian Process Study, together with a description of the behavior of the modeled ecosystem. Stations S04 and S15 are chosen for the comparison, whose locations are shown in Fig. 12. S04 is located close to the coast of Oman and strongly affected by horizontal nitrate transport subsequent to the coastal upwelling caused by SWM. S15 lies in the central Arabian Sea and is not subject to the influence of the coastal upwelling. These stations were also selected as the sites of ecosystem simulation with a vertical one-dimensional model by Kriest (2000).

4.2.1. Comparison near the coast of Oman

Fig. 13 shows the modeled temporal variation of nitrate, chlorophyll, and sinking flux of detritus. The model results have been averaged over a $1^\circ \times 1^\circ$ area centered at station S04. Here, the spatial extent is chosen rather arbitrarily but is not quite different from the first baroclinic Rossby radius at these latitudes (cf., Chelton et al., 1998). In Fig. 13c, the standard deviation (SD) of the simulated particle export within the $1^\circ \times 1^\circ$ area is indicated so that the reader can obtain some sense of fluctuations caused by processes with relatively small scales such as eddies and fronts.

Fig. 13b shows a modest increase of chlorophyll in winter. This is caused by entrainment of underlying nitrate through mixed layer deepening (see Fig. 3). A much more distinct increase is seen during the SWM season. This increase cannot be a direct consequence of the coastal upwelling because Station S04 is located too far away from the coast. To see what process is important in bringing nitrate to the surface, we have calculated the contribution of each term in the governing equation in the top 50 m for the period Jul.–Sep. (figure not shown). In the sum of physical nitrate inputs, namely, those by horizontal/vertical advection/diffusion, horizontal advection accounts for ~ 98% when averaged over the area. Rather surprisingly, horizontal advection of nitrogen in particulate forms, that is, phytoplankton, zooplankton, and detritus, is not negligible at all; the sum of these three contributions even exceeds that of the horizontal advection of nitrate. Therefore, the chlorophyll increase in the SWM season is caused by horizontal transport of nitrogen in both inorganic and organic form following the coastal upwelling along the coast of Oman. Open ocean upwelling through Ekman

Fig. 14. Comparison between the model and observation for (a) nitrate and (b) chlorophyll; solid lines: model, crosses: observation, dashed lines: nitrate climatology by Conkright et al. (1994b) used to initialize the model. The model results are averaged over 16.7–17.7°N, 59.3–60.3°E, and the data are from the station S04 of the U.S.JGOFS Arabian Sea Process Study. The date of observation is indicated above each panel. Corresponding model result is taken from the 10-day period centered at the observation date. Error bars for the model result show the range of the standard deviation within the spatial and temporal extent. The nitrate and chlorophyll data are available at http://www1.whoi.edu/arabian.html by courtesy of Lou Codisposi and Barber et al. (2001), respectively.

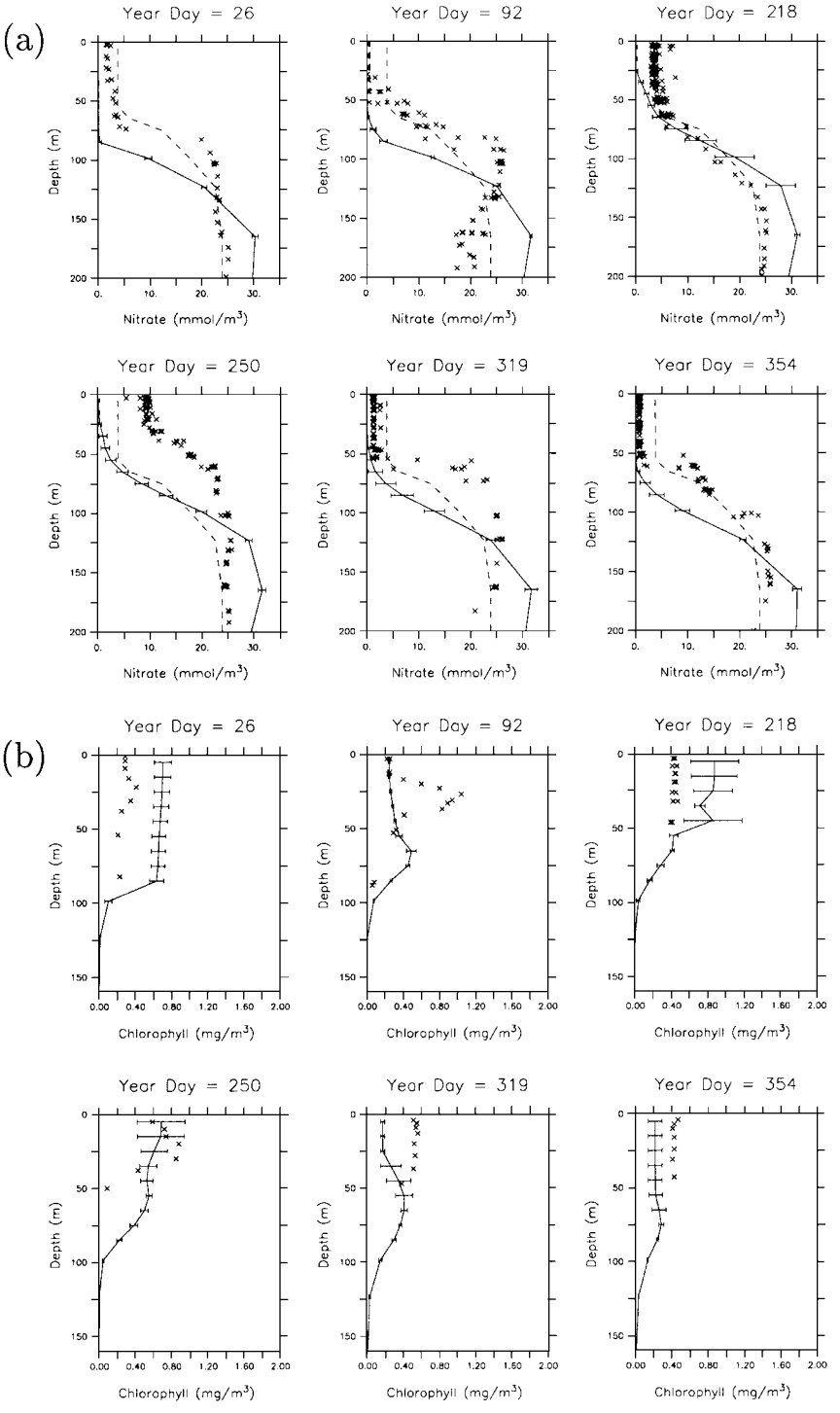
(a)
Year Day = 26
Year Day = 92
Year Day = 218
Year Day = 250
Year Day = 319
Year Day = 354
Depth (m)
Nitrate (mmol/m3)
(b)
Chlorophyll (mg/m3)

divergence is not a major mechanism responsible for the SWM chlorophyll increase at this site in the model. The large SD around the second chlorophyll is a consequence of a distinct front in biological tracers caused by nitrate transport through the coastal upwelling and the subsequent lateral advection (see Figs. 6c and 10a).

A comparison between the model and the observations taken at S04 in 1995 is given in Fig. 14. Model results are retrieved from the area above and a time span of 5 days before and after the date of observation. Averaging has been applied over that period of 10 days as well as over the area. The time scale of 10 days is again a subjective choice, but roughly corresponds to that required for a water particle with a typical advection velocity of 0.1 m/s to pass through the $1^\circ \times 1^\circ$ area. SD within the spatial and temporal extent is shown by the error bars. The simulated chlorophyll concentrations have on average the same magnitude as the observed ones, although large deviations of an order of magnitude occur in the individual profiles. It seems that the model reproduces the nitrate values around the depth of 200 m, although this may be partly because the integration period (8 years) is not long enough to affect nitrate distribution at this depth.

The largest difference between observations and model results is seen in the nitrate profile on day 250, which is in late SWM season. The observed nitrate concentration near the surface is much higher than in the model. Possible causes for this difference include short-term variations in nature or a peculiarity in the year of observation (1995). It seems, however, unlikely that short-term variation is the cause because SD is quite small in the model, though even SD in the model might be underestimated. A peculiarity in the year 1995 does not appear to be the cause either; Shi et al. (2000) found that the upwelling in 1995 was not much stronger than in some other years. We therefore conclude that nitrate transport is not large enough in the model. In this regard, Kawamiya (2001) demonstrated that the model may underestimate lateral nitrate transport to the offshore region by mesoscale currents, whose importance has been demonstrated by Dickey et al. (1998). Interestingly, the discrepancy in the nitrate profile is not reflected in the chlorophyll profile on day 250. The modeled nitrate concentration in the lower euphotic zone is already of the order of the half saturation constant (0.5 mmol/m^3); thus the sensitivity to errors in the simulated nitrate concentration is low. Chlorophyll near the surface is also fairly high because of the horizontal advection of chlorophyll mentioned above.

The observed nitrogen-based detritus flux is shown in Fig. 13c. The original data were taken at a depth of 800 m, and have been converted to the flux in 110 m by applying the empirical equation by Martin et al. (1987):

$$F_{110} = F_{800}(110/800)^{-0.858}, \quad (5)$$

where F_{110} and F_{800} are the fluxes at 110 and 800 m, respectively. This is done because virtually no detritus can reach depths as deep as 800 m in the present model configuration (detritus sinks at a constant speed of 5 m/day and is remineralized at a rate of 0.05/day). Also shown are the data by Buesseler et al. (1998) for the sinking flux across 100 m derived from ^{234}Th measurements. Fig. 13c reveals that the observed values compare well with those from the model, indicating that a reasonable amount of organic matter leaves the surface layer in the model. A sensitivity experiment with a different formulation of detritus sinking will be presented in Section 5.2.

4.2.2. Comparison in the central Arabian Sea

Fig. 15 shows an annual cycle of nitrate, chlorophyll, and sinking flux of detritus averaged over an area 9.5–10.5°N, 64.4–65.4°E corresponding to the station S15. It is seen in Fig. 15a that the nitracline is deepened during SWM. This is primarily due to Ekman downwelling in this season. Corresponding to the movement of the nitracline, the DCM changes its depth (Fig. 15b). Chlorophyll concentrations are

Fig. 15. As in Fig. 13 but for the area 9.5–10.5°N, 64.4–65.4°E corresponding to the station S15; (a) nitrate, (b) chlorophyll, (c) simulated detritus flux at 110-m depth (solid line), observations of particulate organic nitrogen converted to that at 110 m (crosses), and the sinking flux across 100 m derived from ^{234}Th measurements (asterisks). The contour intervals for (a) and (b) and the vertical scale of (c) are the same as in Fig. 13 to facilitate the comparison. The horizontal error bars denote the durations of cruises corresponding to the respective flux data.

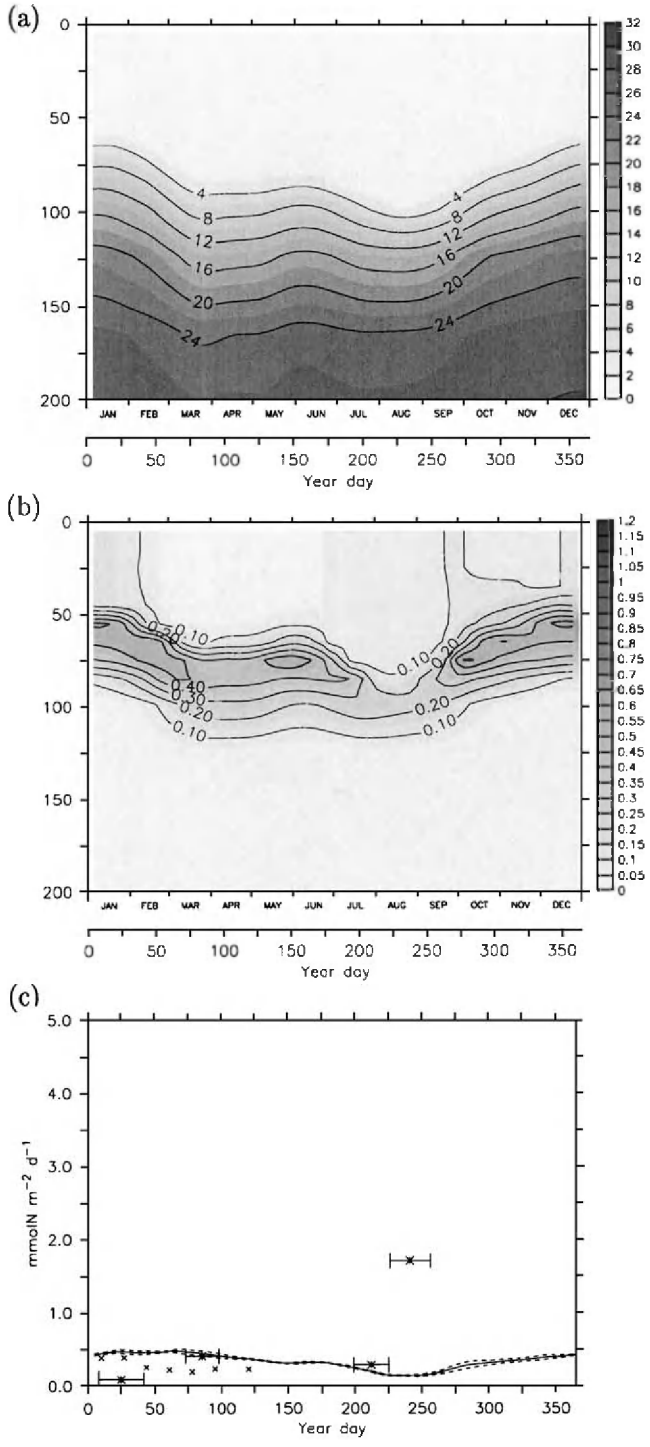
(a)
0
50
100
150
200
JAN FEB MAR APR MAY JUN JUL AUG SEP OCT NOV DEC
0 50 100 150 200 250 300 350
Year day
4
8
12
16
20
24
32 30 28 26 24 22 20 18 16 14 12 10 8 6 4 2 0
(b)
0.10
0.20
0.30
0.40
1.2 1.15 1.1 1.05 1 0.95 0.9 0.85 0.8 0.75 0.7 0.65 0.6 0.55 0.5 0.45 0.4 0.35 0.3 0.25 0.2 0.15 0.1 0.05 0
(c)
mmolN m^{-2} d^{-1}
5.0
4.0
3.0
2.0
1.0
0.0

lowest in August when the nitracline is deepest and thus light conditions for phytoplankton are worst. The sinking flux of detritus is, as expected, much lower than at S04.

A comparison between the model and the data taken at S15 is given in Fig. 16. The model reproduces the observed feature that surface nitrate is depleted throughout the year (Fig. 16a). Agreement can be found also in the depth of the nitracline. A notable difference between model and observations is that the model's vertical nitrate gradient is less steep. This is a rather surprising result considering the fact that the parameter values in the model favor a steep gradient below the nitracline: the sinking velocity is small throughout the water column (5 m/day) and the background vertical mixing coefficient is small as well (0.1 cm^2/s). Indeed, Oschlies et al. (2000), who applied almost the same coupled model to the Atlantic, found that their model often yielded subsurface nitrate concentrations higher than observed. Possible causes for the difference include that the vertical mixing coefficient may be still too high for the Arabian Sea and that the problem of smoothing in the nitrate climatology, used as the initial condition, is more serious in the Arabian Sea than in the Atlantic. Concerning the smoothing problem, it can be seen in Figs. 5, 14a, and 16a) that nitrate gradients in the model are in fact becoming steeper than in the climatology.

The modeled chlorophyll compares rather well with the observation in that it is low near the surface and has a DCM for most of the time. An exception is found at day 211, when the observation shows enhanced surface chlorophyll, whereas the modeled chlorophyll still remains low near the surface. It is possible that the observed increase in chlorophyll is caused by nitrate entrainment following the deepening of the mixed layer in this season. The mixed layer becomes deep in the model as well (Fig. 3), but does not penetrate to the depth where nitrate is abundant enough to stimulate phytoplankton growth. This problem may be associated with that of a too weak gradient in the simulated nitrate profile.

The nitrogen-based detritus flux is shown in Fig. 15c. The model result compares well with the data except for a single point in September, which may reflect the absence of the fall bloom in the central Arabian Sea in this model (see Section 5.1). This relatively good agreement is apparently not in accordance with the fact that the modeled primary production is too low (Fig. 10). This may indicate that the fast recycling discussed in Section 4.1.3 is indeed in effect, since it would increase primary production without much change in the simulated export production.

4.2.3. Nitrogen cycling at the two stations

Seasonal and annual integrals of nitrogen fluxes among the ecosystem compartments are shown in Fig. 17 for the areas corresponding to the two selected stations S04 and S15, so that one can grasp the simulated cycling of nitrogen at the two stations (note the difference in scale between Fig. 17a and b). Fluxes were integrated over the depth range 0–110 m as proxy for the euphotic zone. Here the SWM season is defined as Jun. 1–Sep. 30 and the NEM as Jan. 1–Feb. 28 plus Nov. 1–Dec. 31. SD within the areas is shown by error bars.

In the area around S04, biological activity is most vigorous in the SWM season. As explained in Section 4.2.1, this is primarily due to the horizontal advection of nitrogen, though SD for the horizontal advection of nitrate is even larger than its absolute value when integrated over the upper 110 m. When the integration is performed, as in Section 4.2.1, over the upper 50 m where most phytoplankton grows in the SWM season, SD is considerably smaller. The fact that SD is extremely large is consistent with the ubiquitous existence of mesoscale features in this region close to the energetic coastal jet.

In the area around S15, nitrogen cycling rates are generally smaller than at S04 by a factor of ~ 5. Primary production is lower in the SWM season due to Ekman downwelling prevailing in the central Arabian Sea during this season. In the NEM season, the net sign of nitrate supply by vertical advection is difficult to determine, again due to the effect of mesoscale features. A noticeable feature is that the contribution from horizontal advection of nitrate has always a significant positive value. Horizontal nutrient supply to offshore regions in the Arabian Sea has been a subject of some studies after Banse (1987) postulated that nitrate is transported away from the upwelling region along the coast of Oman (cf., Young and Kindle, 1994; Keen et al., 1997).

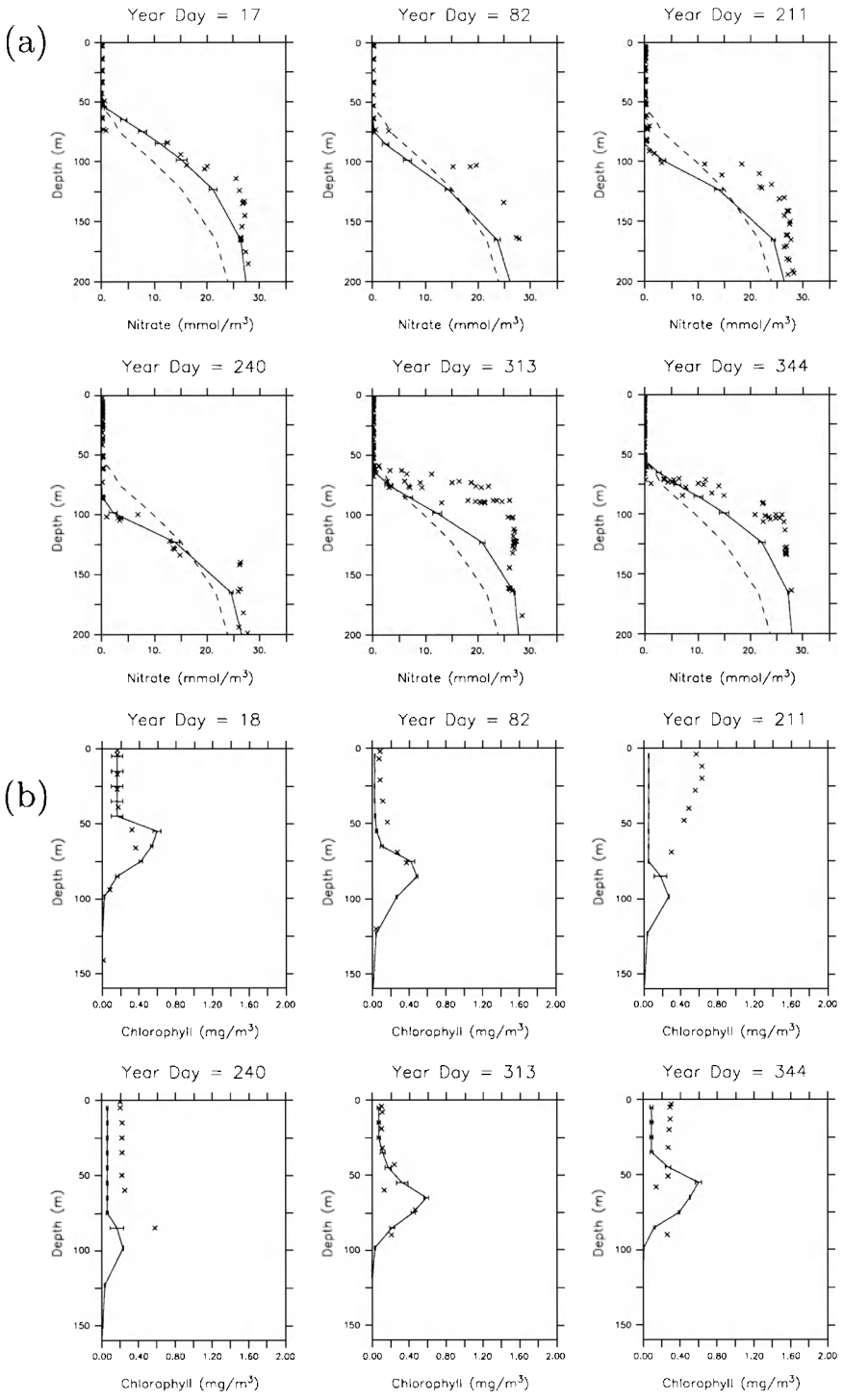

Fig. 16. As in Fig. 14 but for the area 9.5–10.5°N, 64.4–65.4°E, corresponding to S15; (a) nitrate and (b) chlorophyll.

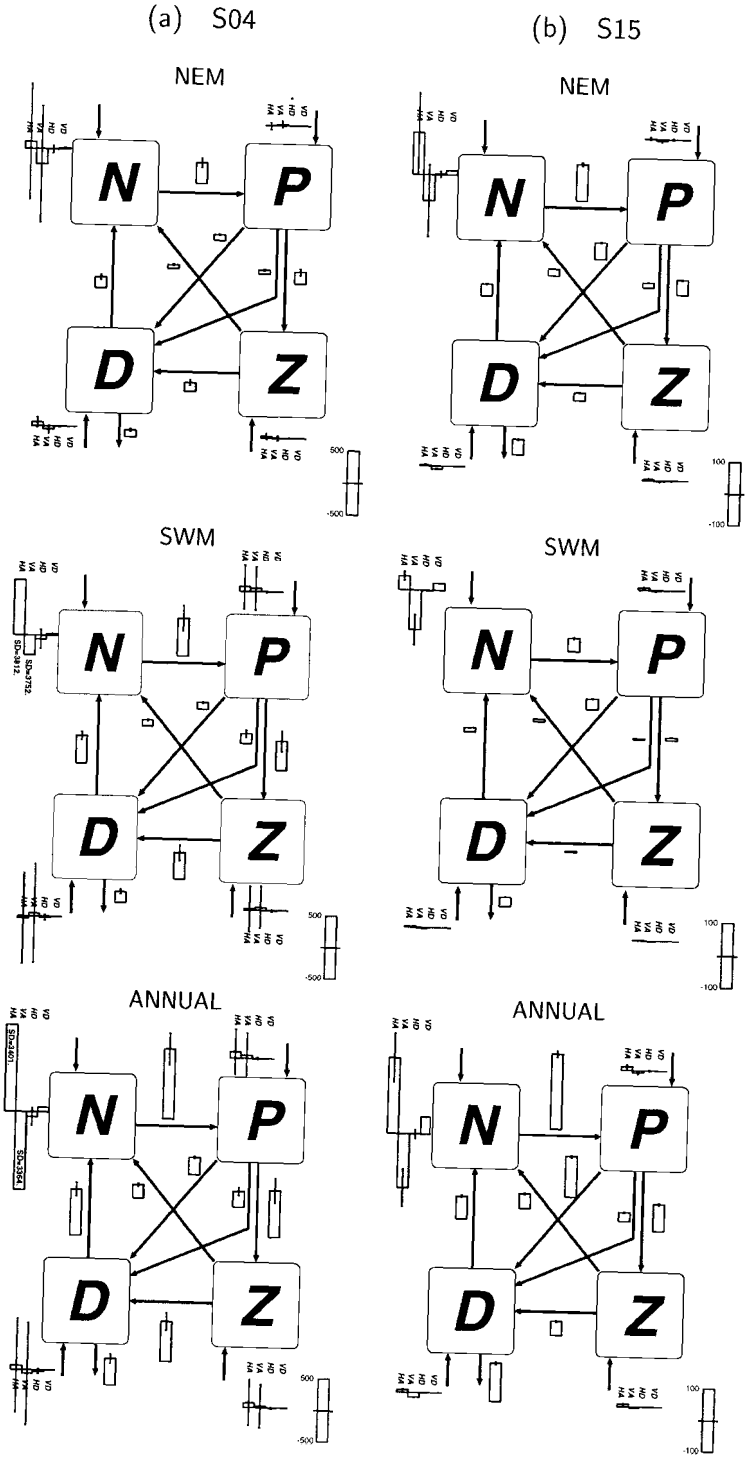
(a) S04
(b) S15
NEM
SWM
ANNUAL
N
P
D
Z

5. Discussion

5.1. Comparison with other models

MKHO and RGF also performed model simulations of the pelagic ecosystem in the Arabian Sea covering an annual cycle. A comparison of the results of the present model with those of the above studies will shed some light on the robustness of the model results. Fig. 18 shows the simulated annual cycles of MLD and the ecosystem compartments in the mixed layer, averaged over the areas in Fig. 12 which have been chosen and named following MKHO. Fig. 18 can be directly compared with Fig. 4 by MKHO and Fig. 1 by RGF.

Common features can be found among the three models such as the long-lasting phytoplankton increase during the SWM season in the areas Somalia and Oman. Among noticeable differences, the most conspicuous one is the absence of the fall bloom in the Central Basin found in both Fig. 4 by MKHO and Fig. 1 by RGF. Satellite measurements of surface chlorophyll are in favor of the existence of the fall bloom (Banse, 1994). MKHO classified this bloom as "detrainment bloom", caused by an abrupt mixed layer shallowing following nutrient accumulation. In the model by RGF, the same type of bloom appears to be occurring in other areas as well. However, the mixed layer shallowing during SWM observed by Dickey et al. (1998) at the WHOI mooring site (15.5°N, 61.5°E) is not large nor abrupt; MLD was ~ 80 m in early July and gradually shoals to ~ 50 m over a month.

The direct cause for the absence of the fall bloom in our model is clearly the lack of the nitrate accumulation preceding the shallowing of the mixed layer. The nitrate concentrations simulated by MKHO and RFG reach as high as ~ 10 mmol/m^3 right before the occurrence of the fall bloom. In turn, this difference seems to result from the mixed layer of our model being shallower than that of MKHO and RGF in the Central Basin during the SWM season. While MLD in our model is ~ 60 m in this season, both the models of MKHO and RGF yield a mixed layer well deeper than 100 m, which is not the case in the observations (see Figs. 3 and 12). On the other hand, the possible underestimation of nitrate supply at S04, pointed out in Section 4.2.1, may lead to underestimate the nitrate concentration in the Central Basin in our model. Indeed, the data by Morrison et al. (1998) show values of ~ 2 mmol/m^3 in the Central Basin during the SWM season, which are between those simulated by our model and by MKHO and RGF. It appears that the nitrate supply in the Central Basin during the SWM season is underestimated in our model and overestimated in their models. In this regard, Kawamiya (2001) reports that the nitrate supply to the offshore region during SWM is mainly achieved through horizontal transport by mesoscale features and that their activity is indeed underestimated by the model.

The model of RGF has a problem similar to that of the overestimated subsurface nitrate maximum in our model. Their Fig. 8 shows that the modeled nitrate concentration is much too high. On the other hand, they do not have the problem of too low primary production (their Fig. 9). Although the cause for the difference with respect to our model results is difficult to identify because of the many differences in physics and biology between the two models, the large vertical mixing coefficient (1.0 cm^2/s) used by RGF may be one reason. The upstream advection scheme they adopted is diffusive as well. Primary production in the oligotrophic regimes is extremely sensitive to vertical diffusivity below the mixed layer. Observations suggest much lower diffusivities (e.g., Ledwell et al., 1993), which are closer to those used in our model (0.1 cm^2/s).

Another conspicuous difference is that zooplankton biomass in our model is higher than that of MKHO by a factor of ~ 4. As RGF discussed, the self-grazing term of zooplankton adopted by MKHO may be one reason for their low zooplankton standing stock.

5.2. Sensitivity experiments

An ecosystem model has typically considerable uncertainty in its configuration and parameter values.

Fig. 17. Seasonal and annual nitrogen fluxes among the compartments of the model ecosystem integrated over the upper 110 m, for the area (a) 16.7–17.7°N, 59.3–60.3°E, corresponding to S04 and (b) 9.5–10.5°N, 64.4–65.4°E, corresponding to S15. Units are in mmolN m^{-2}. Note the difference in scale between (a) and (b). See text for the exact definition of the NEM and SWM season. Error bars show the range of the standard deviation (SD) within the area. Where SD is too large to be displayed with error bars, it is designated with numbers. HA, VA, HD, and VD denote horizontal advection, vertical advection, horizontal diffusion, and vertical diffusion, respectively.

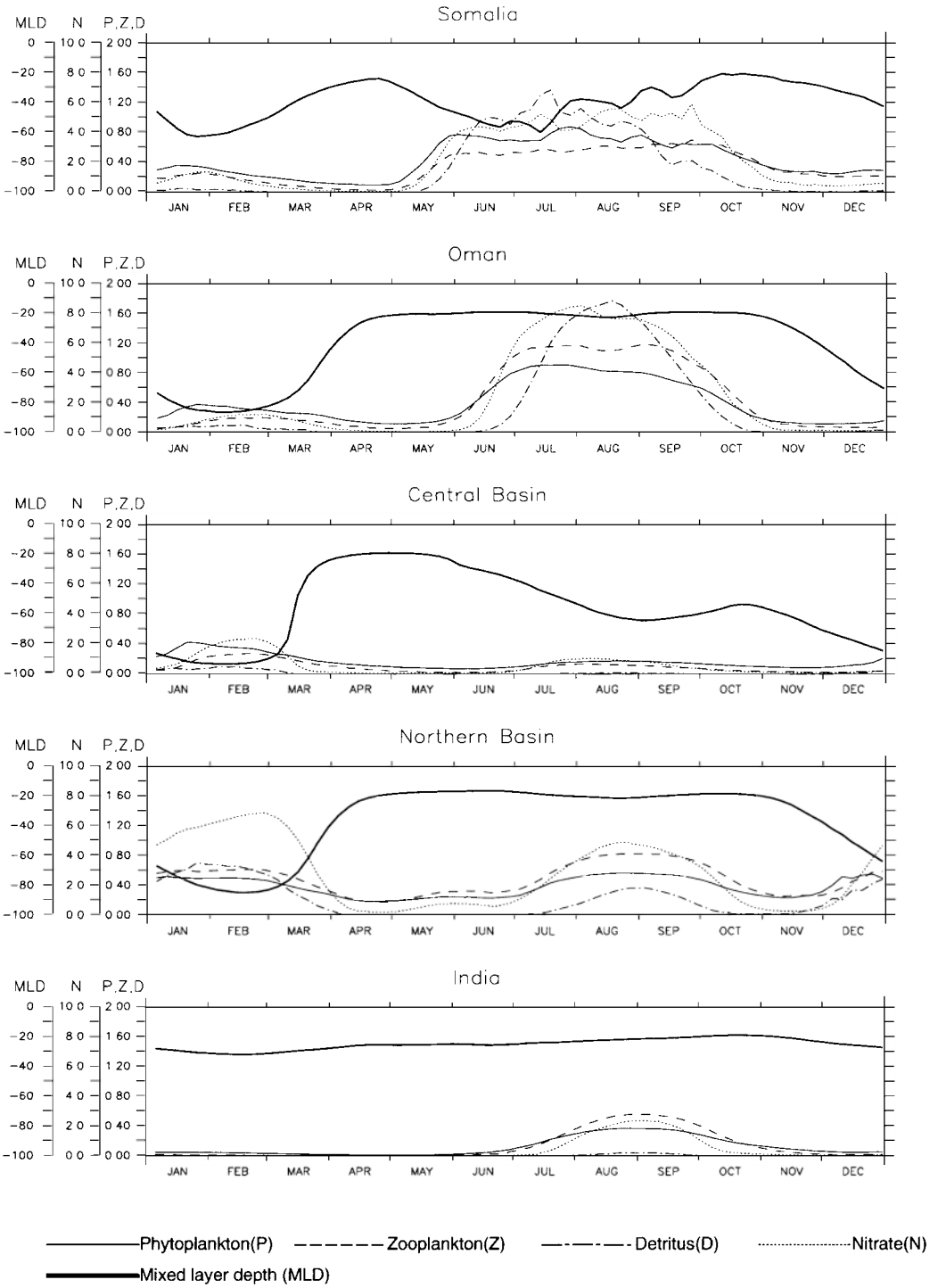

Fig. 18. Temporal evolution of simulated phytoplankton (P), zooplankton (Z), detritus (D), and nitrate (N) averaged over the mixed layer. The mixed layer depth (MLD) is also depicted. Averages have been computed over the areas shown in Fig. 12 for all the variables. Units are in mmol/m^3 for P, Z, D, and N, and in m for MLD.

It is important to carry out sensitivity experiments to check the rigidity of model results. In this section, we carry out four experiments that investigate the model's sensitivities to changes in biological parameters and physical settings.

It turned out that main features of the model results are mostly established already in the third year of integration. Therefore, the model is integrated for only 3 years in the sensitivity experiments, and the results from the third year of integration are compared with those from the standard experiment in the same model year.

5.2.1. Biological parameters

Here, results are shown from sensitivity experiments in which the fast recycling loop introduced by Oschlies (2001) is incorporated and the formulation of detritus sinking is changed.

The fast recycling loop is introduced because drastic improvement was found in simulated primary production in oligotrophic regions in the North Atlantic (Oschlies, 2001). Further pursuing this issue, Oschlies (2002) compared the surface heat flux diagnosed from the model with data. The result indicated that over the oligotrophic subtropical gyre of the North Atlantic, the simulated downward heat transport is relatively large compared with observations, suggesting that upward nitrate flux would also be large. Together with direct comparisons of upward nitrate flux at two points where observations have been carried out, he concluded that the model already provides enough upward flux of nitrogen even in oligotrophic regions. Kriest (2000) performed experiments with a one-dimensional model for both eutrophic and oligotrophic sites in the Arabian Sea. The results also suggest that a fast recycling is necessary to reproduce observed high primary production rates. Concerning the formulation of detritus sinking, it has been pointed out by Oschlies et al. (2000) that the detritus sinking velocity in this model (5 m/day) may be too small. The focus will be on the two major basin-scale problems, that is, the subsurface nitrate maximum in the northern end of the Arabian Sea, and the too low primary productivity in oligotrophic regimes.

In the first sensitivity experiment, a nitrogen return flow from phytoplankton to nitrate is added to the structure shown in Fig. 1, and the linear function for the phytoplankton loss to detritus is replaced by a quadratic one (Oschlies, 2001). The nitrogen flow from phytoplankton to nitrate is proportional to the modeled phytoplankton abundance with the rate 0.05/day, and the quadratic mortality rate is set to 0.05 $\mathrm{mmol}^{-1}\ \mathrm{m}^3\ \mathrm{day}^{-1}$. In the second sensitivity experiment in which the nitrogen flows are returned exactly to the one in Fig. 1, the detritus sinking velocity is increased to 10 m/day above 144-m depth. Below that depth, the equation by Martin et al. (1987) is adopted to describe the vertical profile of the detritus sinking flux:

$$F = F_{144}\left(\frac{z}{144}\right)^{-0.858}, \tag{6}$$

where F is the detritus sinking flux as a function of depth, F_{144} the detritus sinking flux at 144-m depth, and z is the depth in meters. This formulation implies that a certain portion of the detritus flux across 144-m depth can reach the bottom immediately. The downward transport of detritus is much faster than in the standard run, and can thus be expected to relief the unrealistic nitrate maximum. This treatment of the detritus sinking process is quite similar to that employed by Sarmiento et al. (1993) and Fasham et al. (1993). For the sensitivity experiments, the model was integrated in the same way as described in Section 2.3, and the results for nitrate distribution and primary production in the third year are displayed in Fig. 19c–f, along with those from the standard experiment in the same year (Fig. 19a and b).

In the experiment with the fast recycling loop, primary production in oligotrophic regimes becomes indeed higher by a factor of 2 to 3. The simulated values are still substantially lower than those of Antoine et al. (1996), but fairly close to those of Behrenfeld and Falkowski (1997) (Fig. 10b and c). The annual export ratio calculated at 110-m depth (0.095) is now within the range of the observation-based estimates by Lee et al. (1998) and Buesseler et al. (1998) (~ 0.25 for SWM, ~ 0.05 for other seasons). The fast recycling loop is meant to embody the notion that small-size species of phytoplankton tend to dominate the ecosystem in an oligotrophic regime, thereby reducing the sinking velocity averaged over the whole size spectrum. Though it is not very clear if such behavior of the ecosystem is ubiquitous and if it is faithfully represented by the

fast recycling loop we introduced, it is instructive that such a moderate change in the model configuration can considerably alter the simulated primary production.

Although the fast recycling loop is likely to be important to close the gap between the modeled and observation-based primary production, the increase in primary production in the Arabian Sea is not as

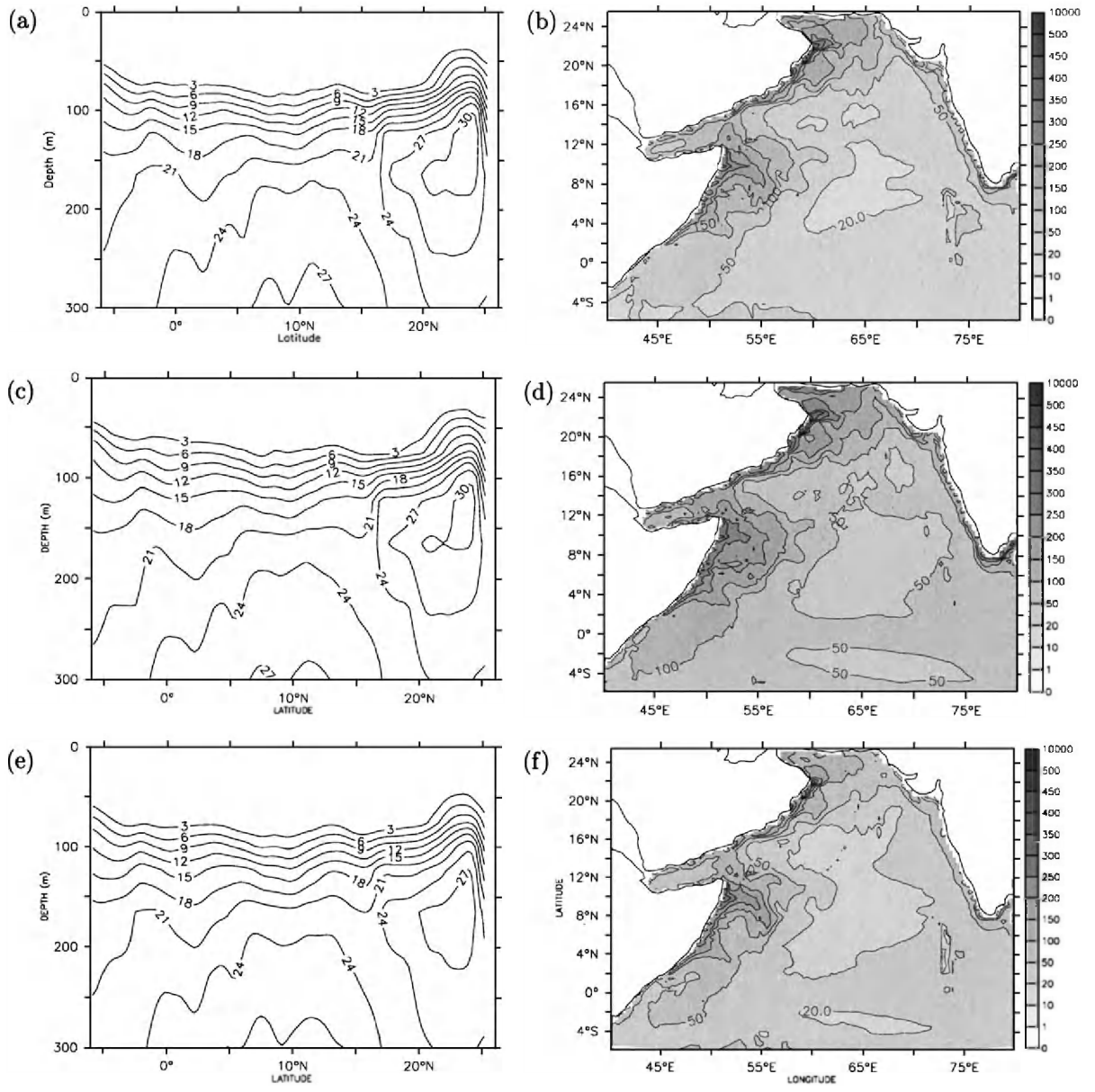

Fig. 19. Model results in the third year of integration for (a,c,e,g,i) annual mean nitrate along 65°E and (b,d,f,h,j) annual primary production from different experiments with (a,b) the standard configuration, (c,d) the fast recycling loop, (e,f) the detritus sinking formulation by Martin et al. (1987), (g,h) wind stress by daSilva et al. (1994), and (i,j) the mixed layer model by Gaspar et al. (1990).

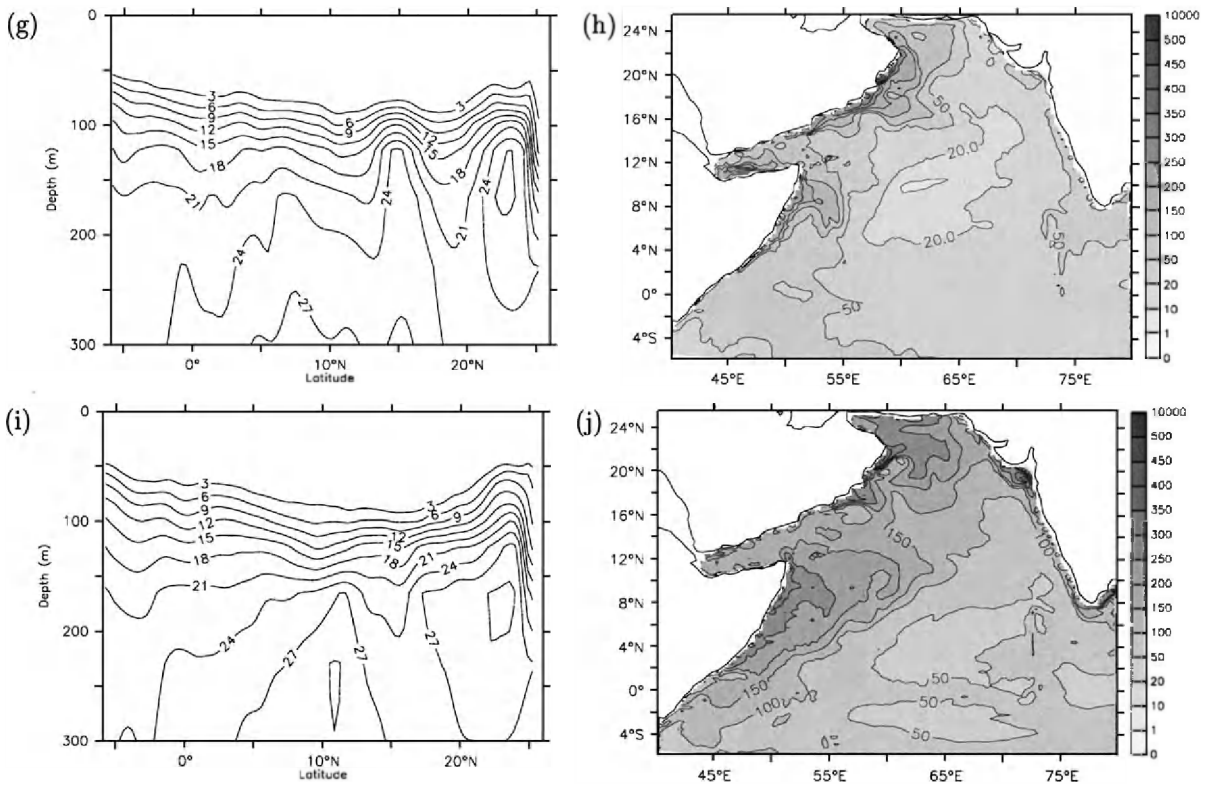

Fig. 19 (*continued*).

dramatic as in the North Atlantic where it was more than an order of magnitude (Oschlies, 2001). This is because the depths of the nitracline in oligotrophic regimes are shallower in the Arabian Sea, thereby supplying significant nitrate to fuel phytoplankton growth near the bottom of the euphotic zone even without the fast recycling loop.

With the faster sinking of detritus, annual primary production is reduced by 33% (Fig. 19f). The concentrations in the subsurface nitrate maximum are also reduced by ~ 2 mmol/m^3 (Fig. 19e). This is caused both by the more efficient removal of detritus from the subsurface layer and by the smaller amount of detritus formation in the surface layer due to the reduction in primary production. However, the reduction is too small to eliminate the unrealistic nitrate maximum. As discussed in Section 4.1.1, it is thus probable that this maximum is a result of the neglect of denitrification and not of the particular settings of the ecosystem model.

5.2.2. Physical settings

We saw in Section 3.2 that the location of the maximum MLD in August is shifted southward compared to the climatology (Fig. 3). Its exact location may be partly determined by the Ekman downwelling, which prevails in the central part of the Arabian Sea during the SWM. The distribution and strength of the Ekman downwelling in the model are in turn determined by the wind stress field applied. Also, the particular choice of a vertical mixing scheme can be critical for the simulated MLD. In the following, we show results from sensitivity experiments with respect to these physical settings.

Fig. 20c and d depict the MLD for January and August, respectively, in the experiment where the wind forcing data are switched to those by daSilva et al. (1994). Corresponding plots from the standard experiment are shown in Fig. 20a and b. Although the MLD maximum in August is slightly moved northward in this sensitivity experiment, it is still located to the south

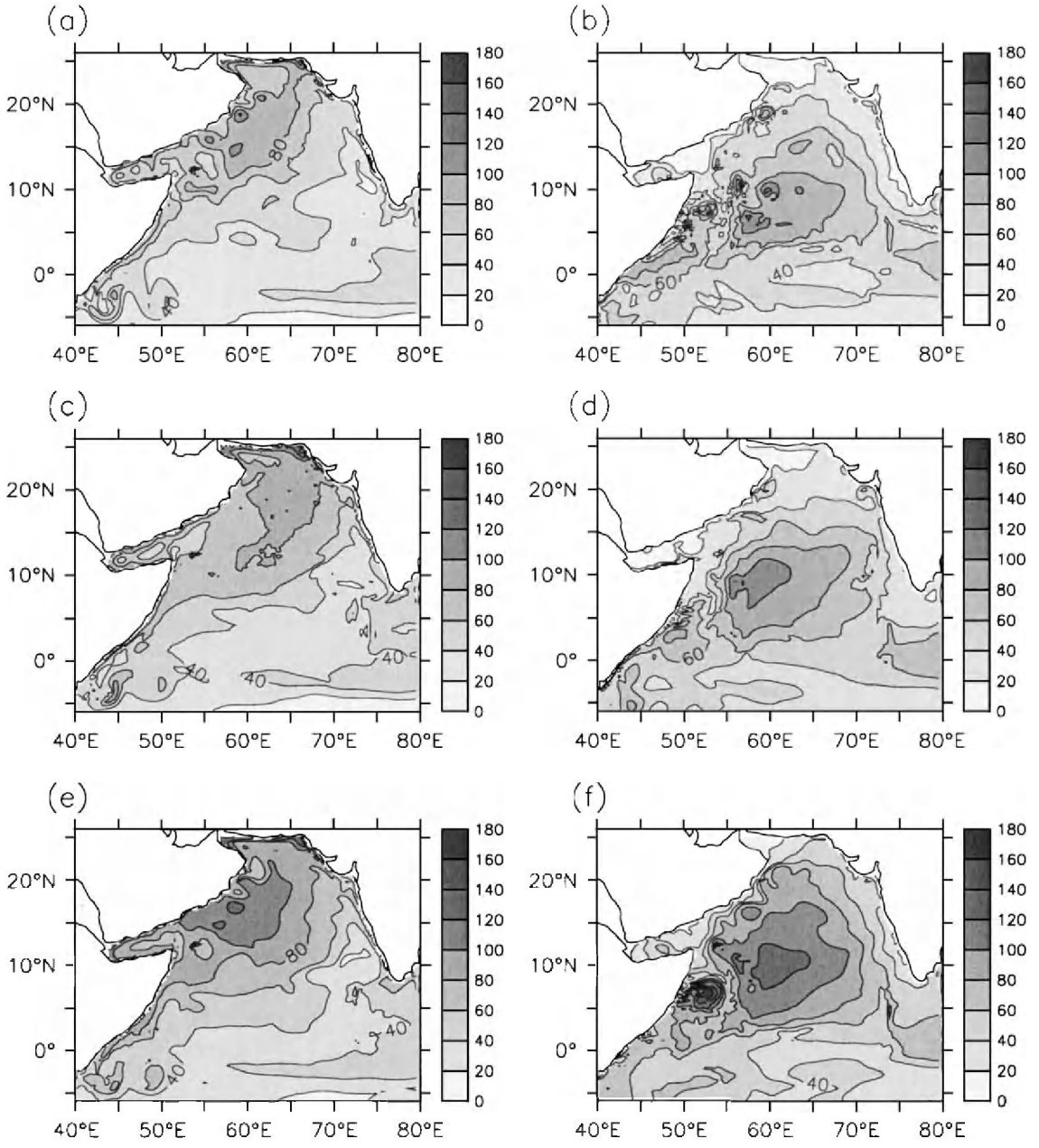

Fig. 20. Mixed layer depth in the third year of integration for the model averaged over (a,c,e) January and (b,d,f) August from different experiments with (a,b) the standard configuration, (c,d) wind stress by daSilva et al. (1994), and (e,f) the mixed layer model by Gaspar et al. (1990).

of that in the climatology. In January, the mixed layer becomes shallower than in the standard experiment by ~ 20 m near the coast of Oman. This difference is caused by mesoscale features. Along the coast of Oman, warm-core rings are constantly found in both experiments but are more energetic in the standard experiment. This leads to a weaker stratification and thus a deeper mixed layer in the standard experiment,

because warm-core rings are associated with downward excursion of isotherms.

The overall distributions of nitrate and primary production are essentially unaffected by a change in the wind field (Fig. 19g and h). The problem of the unrealistic nitrate maximum is, however, eased visibly. This is because the wind-driven transport of nitrate from the upwelling region along the coast of Oman to the northern end of the Arabian Sea is reduced in this sensitivity experiment. This results in a lower primary productivity in the northern end of the Arabian Sea leading to a weaker source of remineralized nitrate for the subsurface layer.

The model yields the MLDs displayed in Fig. 20e and f when the vertical mixing scheme by Pacanowski and Philander (1981) is replaced by the mixed layer model of Gaspar et al. (1990) as adapted by Blanke and Delecluse (1993). This mixed layer model calculates the vertical diffusivity and viscosity from the turbulent kinetic energy (TKE), for which a prognostic equation is solved. The only changes made with respect to the implementation by Blanke and Delecluse (1993) are a surface boundary condition (SBC) for TKE ($\bar{e}$) and the lower limit of TKE; the SBC is now $K_e \partial \bar{e}/\partial z = 3u_*^3$ where K_e is the vertical diffusivity for TKE and u_* the friction velocity, and the minimum TKE is set to 4×10^{-2} cm^2/s^2 (Oschlies and Garçon, 1999). The MLDs are deeper than in the standard experiment by $\sim$ 20 m in January, thereby making the deviation from the climatology of Fig. 3c slightly larger. In August, the MLDs are 20–40 m deeper than in the standard experiment, and the maximum value is now larger than that in the climatology of Fig. 3d but similar to that in the MLD climatology by Rao et al. (1989). In the northern part, however, mixed layers are deeper than in the Rao et al. (1989) data by 30–40 m in August, whereas the standard experiment bears better resemblance there. Overall, it is not clear which of the MLDs in the two experiments is closer to reality.

The vertical diffusivity below the mixed layer is also enhanced from 0.1 cm^2/s in the standard experiment to $\sim$ 0.3 cm^2/s in this experiment due to the nature of the Gaspar et al. (1990) mixed layer model, which provides diffusivities proportional to the reciprocal of the Brunt-Väisälä frequency in stably stratified regions. These moderate changes in the MLD and vertical diffusivity cause a drastic change in the annual primary production field (Fig. 19j). The deeper mixed layer enables more nitrate entrainment, thereby enhancing primary production to the extent that the values are similar to those in the satellite-based estimate by Behrenfeld and Falkowski (1997), although lower than those by Antoine et al. (1996) (Fig. 10b and c). The simulated spatial pattern resembles that of the satellite-based estimates. The enhancement of primary production is seen throughout the year, and is especially strong in the SWM season. The annual export ratio calculated at 110-m depth remains rather high (0.38) compared to the observation-based estimates by Lee et al. (1998) and Buesseler et al. (1998) ($\sim$ 0.25 for SWM, $\sim$ 0.05 for other seasons). Sinking fluxes across 110 m at S04 and S15 are higher than those observed by a factor of 2–3 (figures not shown). Correspondingly, the subsurface nitrate maximum takes on even higher values (Fig. 19i).

The increasing rate in integrated nitrate content is calculated over the domain to the north of 10°N and down to 670-m depth for all the sensitivity experiments presented here, and ranges from 11 TgN/year in the experiment with the Martin et al. (1987) curve to 24 TgN/year in that with the Gaspar et al. (1990) mixed layer model. This may give an idea on the uncertainty of the model-based denitrification rate evaluated in Section 4.1.1.

6. Summary and outlook

A nitrogen-based, four-compartment ecosystem model has been coupled into an eddy-permitting ocean general circulation model for the entire Indian Ocean. A second-order advection scheme, which bears much less computational diffusion than upstream differentiation, is used for the biological variables. The coupled model has been integrated for 8 years after spinning up the physical model. Comparison between the model results and the observations shows that the model reproduces many features observed in reality in both physical and biological variables, e.g., the deep summer mixed layer in the central Arabian Sea, the increase in chlorophyll concentration during the SWM season along the coast of Oman and Somalia, and the shoaling of nitracline toward the north.

Two major differences are found in the basin-wide comparison between the model results and the observations. One is that the model produces an unrealistic

subsurface nitrate maximum in the northern end of the Arabian Sea, and the other is that the simulated primary production is too low in oligotrophic regimes. A comparison with in situ data reveals that the model sometimes simulates a too weak gradient of nitrate profile in spite of the present model configuration being favorable for a strong nitrate gradient. The sinking flux of detritus out of the euphotic zone shows good agreement when extrapolated data are used, leaving an apparent inconsistency between the model's too low primary productivity and sufficient sinking flux in oligotrophic regimes.

The problem of subsurface nitrate maximum is probably caused by the fact that the model lacks the denitrification process. Nitrate is increasing in the maximum region with a rate of 11–24 TgN/year. This number may be used as a model-based indirect estimate for the denitrification rate integrated over the northern Arabian Sea if the nitrogen lost through denitrification is compensated by lateral advection of nitrate, as suggested by Bange et al. (2000). Investigation of this subsurface maximum may provide some insight into the denitrification process taking place in almost the same area in reality.

The cause for the problem of too low primary production is not clear, while fast recycling of nitrate, carbon fixation decoupled from nitrogen, and nitrogen fixation have been proposed as possible explanations. The fast recycling loop of nitrogen adopted by Oschlies (2001) has been introduced in the model and showed an increase by a factor of 2 to 3 in oligotrophic regions. Considering that the model works well regarding the sinking flux out of the euphotic zone and that the required increase in simulated primary production should thus be accomplished through regenerated production, the fast recycling may be happening in reality.

Changing the vertical mixing scheme by Pacanowski and Philander (1981) to that by Gaspar et al. (1990) also increases primary production and yields an even better agreement of the spatial pattern than in the experiment with the fast recycling loop. Sinking fluxes are, however, larger than in observations by a factor of 2–3. It cannot be assertively concluded which of the fast recycling loop and the adoption of the TKE model can better cure the problem. The drastic changes are impressing when one takes into account that the changes in the MLD are not extremely large (20–40 m deeper with the Gaspar et al., 1990 scheme). The choice of a vertical mixing scheme may be more critical in the Arabian Sea than in other basins such as the North Pacific where the patterns of biological variables are primarily determined by the Ekman upwelling field.

Comparison with the models by McCreary et al. (1996) and Ryabchenko et al. (1998) shows that our model does not produce a phytoplankton bloom in the late SWM season, while both of the other two models do. This is because nitrate does not accumulate in the relatively deep mixed layer during summer in our model. In turn, possible reasons for the lack of nitrate accumulation are that the mixed layer may be too shallow in summer and that horizontal transport of nitrate from the coast of Oman may be too weak. The mechanism for the bloom should be investigated in more detail by both modeling and observations.

After identifying the model's ability and inability, the model can be applied to more practical issues such as interannual variability of the ecosystem, mechanism of nitrate supply during the SWM bloom (Kawamiya, 2001), and seasonal variation of export ratio (Kawamiya and Kriest, submitted for publication), taking enough care of the model's deficiencies.

Acknowledgements

This study is a contribution to the German JGOFS program. The authors are grateful to Nils Rix for setting up the physical model. Special thanks are given to Iris Kriest for the discussion and the pre-processing of observational data. The discussion with Wolfgang Barkmann, Achim Wirth, Jürgen Willebrand, and Bernt Zeitzschel has been always stimulating. The software FERRET was extensively used for the analysis and graphics.

References

Antoine, D., André, J.-M., Morel, A., 1996. Oceanic primary production: 2. Estimation at global scale from satellite (Coastal Zone Color Scanner) chlorophyll. Glob. Biogeochem. Cycles 10, 57–69.

Antonov, J.I., Levitus, S., Boyer, T.P., Conkright, M.E., O'Brien, T.D., Stephens, C., 1998. NOAA Atlas NESDIS 29, World

Ocean Atlas 1998, vol. 3: Temperature of the Indian Ocean. Tech. rep., NODC.

Bange, H.W., Rixen, R., Johansen, A.M., Siefert, R.L., Ramesh, R., Ittekkot, V., Hoffmann, M.R., Andreae, M.O., 2000. A revised nitrogen budget for the Arabian Sea. Glob. Biogeochem. Cycles 14, 1283–1297.

Banse, K., 1987. Seasonality of phytoplankton chlorophyll in the central and northern Arabian Sea. Deep-Sea Res. 34, 713–723.

Banse, K., 1994. On the coupling of hydrography, phytoplankton, zooplankton, and settling organic particles offshore in the Arabian Sea. In: Lal, D. (Ed.), Biogeochemistry of the Arabian Sea. Indian Academy of Science, Bangalore, pp. 27–63.

Barber, R.T., Marra, J., Bidigare, R.C., Codispoti, L.A., Halpern, D., Johnson, Z., Latasa, M., Goericke, R., Smith, S.L., 2001. Primary productivity and its regulation in the Arabian Sea during 1995. Deep-Sea Res. II 48, 1127–1172.

Barnier, B., Siefridt, L., Marchesiello, P., 1995. Surface thermal boundary condition for a global ocean circulation model from a three-year climatology of ECMWF analysis. J. Mar. Syst. 6, 363–380.

Behrenfeld, M.J., Falkowski, P.G., 1997. Photosynthetic rates derived from satellite-based chlorophyll concentration. Limnol. Oceanogr. 42, 1–20.

Blanke, B., Delecluse, P., 1993. Variability of the tropical Atlantic ocean simulated by a general circulation model with two different mixed-layer physics. J. Phys. Oceanogr. 23, 1363–1388.

Boyer, T.P., Levitus, S., Antonov, J.I., Conkright, M.E., O'Brien, T.D., Stephens, C., 1998. NOAA Atlas NESDIS 32, World Ocean Atlas 1998, vol. 6: Salinity of the Indian Ocean. Tech. Rep., NODC.

Brock, J.C., McClain, C.R., 1992. Interannual variability in phytoplankton blooms observed in the northwestern Arabian Sea during the southwest monsoon. J. Geophys. Res. 97, 733–750.

Buesseler, K., Ball, L., Andrews, J., Benitez-Nelson, C., Belastock, R., Chai, F., Chao, Y., 1998. Upper ocean export of particulate organic carbon in the Arabian Sea derived from thorium-234. Deep-Sea Res. II 45, 2461–2487.

Chelton, D.B., deSzoeke, R.A., Schlax, M.G., 1998. Geographical variability of the first baroclinic Rossby radius of deformation. J. Phys. Oceanogr. 28, 433–460.

Conkright, M.E., Levitus, S., Boyer, T.P., 1994a. World Ocean Atlas 1994. vol. 1 of NOAA Atlas NESDIS. NODC.

Conkright, M.S., Levitus, S., Boyer, T.P., 1994b. NOAA Atlas NESDIS 1: World Ocean Atlas 1994, vol.1, Nutrients. Tech. Rep., NODC.

Conkright, M.E., O'Brien, T.D., Levitus, S., Boyer, T.P., Stephens, C., Antonov, J.I., 1998. World Ocean Atlas 1998. vol. 12 of NOAA Atlas NESDIS. NODC.

daSilva, A.M., Yong, C.C., Levitus, S., 1994. Atlas of Surface Marine Data. NOAA Atlas NESDIS US Department of Commerce, Washington, DC.

Dickey, T., Marra, J., Sigurdson, D.E., Weller, R.A., Kinkade, C.S., Zedler, S.E., Wiggert, J.D., Langdon, C., 1998. Seasonal variability of bio-optical and physical properties in the Arabian Sea: October 1994–October 1995. Deep-Sea Res. II 45, 2001–2025.

Eppley, R.W., 1972. Temperature and phytoplankton growth in the sea. Fish. Bull. 70, 1063–1085.

Evans, G.T., Parslow, J.S., 1985. A model of annual plankton cycles. Biol. Oceanogr. 3 (2), 327–347.

Fasham, M.J.R., 1995. Variations in the seasonal cycle of biological production in subarctic oceans: a model sensitivity analysis. Deep-Sea Res. 42, 1111–1149.

Fasham, M.J.R., Sarmiento, J.L., Slater, R.D., Ducklow, H.W., Williams Jr., R. 1993. Ecosystem behavior at Bermuda Station S and Ocean Weather Station INDIA: an observational analysis. Glob. Biogeochem. Cycles 7 (2), 379–415.

Gallacher, P.C., Rochford, P.A., 1995. Numerical simulations of the Arabian Sea using tracers as proxies for phytoplankton biomass. J. Geophys. Res. 100, 18565–18579.

Gaspar, P., Grégoris, Y., Lefevre, J.-M., 1990. A simple eddy kinetic energy model for simulations of the oceanic vertical mixing: tests at Station Papa and Long-Term Upper Ocean Study site. J. Geophys. Res. 95, 16179–16193.

Gunson, J., Oschlies, A., Garçon, V., 1999. Sensitivity of ecosystem parameters to simulated satellite ocean color data using a coupled physical–biological model of the North Atlantic. J. Mar. Res. 57, 613–639.

Haney, R.L., 1971. Surface thermal boundary condition for ocean circulation models. J. Phys. Oceanogr. 1, 241–248.

Howell, E.A., Doney, S.C., Fine, R.A., Olson, D.B., 1997. Geochemical estimates of denitrification in the Arabian Sea and the Bay of Bengal during WOCE. Geophys. Res. Lett. 24, 2549–2552.

Hurtt, G.C., Armstrong, R.A., 1996. A pelagic ecosystem model calibrated with BATS data. Deep-Sea Res. II 43, 653–683.

Jerlov, N.G., 1968. Optical Oceanography. Elsevier, Amsterdam, 194 pp.

Karl, D.M., Hebel, D.V., Björkman, K., Letelier, R.M., 1998. The role of dissolved organic matter release in the productivity of the oligotrophic North Pacific Ocean. Limnol. Oceanogr. 43, 1270–1286.

Kawamiya, M., 2001. Mechanism of offshore nutrient supply in the western Arabian Sea. J. Mar. Res. 59, 675–696.

Kawamiya, M., Kriest, I., 2002. Seasonal variation of export ratio in the Arabian Sea predicted by an ecosystem-circulation model with particle aggregation. Deep-Sea Res. (submitted for publication).

Kawamiya, M., Kishi, M.J., Suginohara, S., 2000a. An ecosystem-physical combined model for the North Pacific: Part I. Model description and the characteristics of the spatial distributions of biological variables. J. Mar. Syst. 25, 129–157.

Kawamiya, M., Kishi, M.J., Suginohara, S., 2000b. An ecosystem-physical combined model for the North Pacific: Part II. Mechanisms of the seasonal variation of chlorophyll. J. Mar. Syst. 25, 159–178.

Keen, T.R., Kindle, J.C., Young, D., 1997. The interaction of southwest monsoon upwelling, advection and primary production in the northwest Arabian Sea. J. Mar. Syst. 13, 61–82.

Kriest, I., 2000. Modelling biogeochemical processes in the Arabian Sea. No. 162. Berichte aus dem Fachbereich Geowissenschaften der Universität Bremen. Bremen (September), 38 pp.

Lafore, J.P., et al., 1998. The Meso-NH atmospheric simulation system: I. Adiabatic formulation and control simulations. Ann. Geophys. 16, 90–109.

Latasa, M., Bidigare, R.R., 1998. A comparison of phytoplankton populations of the Arabian Sea during the Spring Intermonsoon Southwest Monsoon of 1995 as described by HPLC-analyzed pigments. Deep-Sea Res. II 45, 2133–2170.

Ledwell, J.R., Wilson, A.J., Low, C.S., 1993. Evidence for slow mixing across the pycnocline from an open-ocean tracer release experiment. Nature 364, 701–703.

Lee, C., Murray, D.W., Barber, R.T., Buesseler, K.O., Dymond, J., Hedges, J.I., Honjo, S., Manganini, S.J., Marra, J., Moser, C., Peterson, M.L., Prell, W.L., Wakeham, S.G., 1998. Particulate organic carbon fluxes: compilation of results from the 1995 US JGOFS Arabian Sea Process Study. Deep-Sea Res. II 45, 2489–2501.

Levitus, S., Boyer, T.P., 1994a. NOAA Atlas NESDIS 3: World Ocean Atlas 1994, vol. 3, Salinity. Tech. Rep., NODC.

Levitus, S., Boyer, T.P., 1994b. NOAA Atlas NESDIS 4: World Ocean Atlas 1994, vol. 4, Temperature. Tech. Rep., NODC.

Longhurst, A., 1995. Seasonal cycles of pelagic production and consumption. Prog. Oceanogr. 36, 77–167.

Longhurst, A., Sathyendranath, S., Platt, T., Caverhill, C., 1995. An estimate of global primary production in the ocean from satellite radiometer data. J. Plankton Res. 17, 1245–1271.

Mantoura, R.F.C., Law, C.S., Owens, N.J.P., Llewellyn, P.C.A., 1993. Nitrogen biogeochemical cycling in the northwestern Indian Ocean. Deep-Sea Res. II, 651–671.

Martin, J.H., Knauer, G.A., Karl, D.M., Broenkow, W.W., 1987. VERTEX: carbon cycling in the northeast Pacific. Deep-Sea Res. 34, 267–285.

McCarthy, J.J., Garside, C., Nevins, J.L., 1999. Nitrogen dynamics during the Arabian Sea northeast monsoon. Deep-Sea Res. II 46, 1623–1664.

McCreary, J.P., Kohler, K.E., Hood, R.R., Olson, D.B., 1996. A four-compartment ecosystem model of biological activity in the Arabian Sea. Prog. Oceanogr. 37, 193–240.

McCreary, J.P., Kohler, K.E., Hood, R.R., Smith, S., Kindle, J., Fischer, A.S., Waller, R.A., 2001. Influences of diurnal and intraseasonal forcing on mixed-layer and biological variability in the central Arabian Sea. J. Geophys. Res. 106, 7139–7155.

McGillicuddy, D.J., Robinson, A.R., Siegel, D.A., Jannasch, H.W., Johnson, R., Dickey, T.D., McNeil, J., Michaels, A.F., Knap, A.H., 1998. Influence of mesoscale eddies on new production in the Sargasso Sea. Nature 394, 263–266.

Morrison, J.M., Codispoti, L.A., Gaurin, S., Jones, B., Manghnani, V., Zheng, Z., 1998. Seasonal variation of hydrographic and nutrient fields during the US JGOFS Arabian Sea Process Study. Deep-Sea Res. II 45, 2053–2101.

Morrison, J.M., Codispoti, L.A., Smith, S.L., Wishner, K., Flagg, C., Gardner, W.D., Gaurin, S., Naqvi, S.W.A., Manghnani, V., Prosperie, L., Gundersen, J.S., 1999. The oxygen minimum zone in the Arabian Sea during 1995. Deep-Sea Res. II 46, 1903–1931.

Naqvi, S.W.A., 1987. Some aspects of the oxygen-deficient conditions and denitrification in the Arabian Sea. J. Mar. Res. 45, 1049–1072.

Naqvi, S.W.A., 1994. Denitrification processes in the Arabian Sea. In: Lal, D. (Ed.), Biogeochemistry of the Arabian Sea. Indian Academy of Sciences, Bangalore, pp. 181–202.

Naqvi, S.W.A., Shailaja, M.S., 1993. Activity of the respiratory electron transport system and respiration rates within the oxygen minimum layer of the Arabian Sea. Deep-Sea Res. II 40, 687–695.

Oschlies, A., 2001. Model-derived estimates of new production: new results point towards lower values. Deep-Sea Res. II 48, 2173–2197.

Oschlies, A., 2002. Nutrient supply to the surface waters of the North Atlantic: a model study. J. Geophys. Res. 107 (10.1029/2000JC000275).

Oschlies, A., Garçon, V., 1998. Eddy-induced enhancement of primary production in a model of the North Atlantic Ocean. Nature 394, 266–269.

Oschlies, A., Garçon, V., 1999. An eddy-permitting coupled physical–biological model of the North Atlantic 1. Sensitivity to advection numerics and mixed layer physics. Glob. Biogeochem. Cycles 13, 135–160.

Oschlies, A., Koeve, W., Garçon, V., 2000. An eddy-permitting coupled physical–biological model of the North Atlantic 2. Ecosystem dynamics and comparison with satellite and JGOFS local studies data. Glob. Biogeochem. Cycles 14, 499–523.

Pacanowski, R.C., 1995. MOM 2 documentation, user's guide and reference manual. Tech. Rep. 3, GFDL Ocean.

Pacanowski, R.C., Philander, S.G.H., 1981. Parameterization of vertical mixing in numerical models of tropical oceans. J. Phys. Oceanogr. 11, 1443–1451.

Paulson, C.A., Simpson, J.J., 1977. Irradiance measurements in the upper ocean. J. Phys. Oceanogr. 7, 952–956.

Prunet, P., Minster, J.-F., Echevin, V., Dadou, I., 1996a. Assimilation of surface data in a one-dimensional physical–biogeochemical model of the surface ocean: 2. Adjusting a simple trophic model to chlorophyll, temperature, nitrate, and pCO_2 data. Glob. Biogeochem. Cycles 10, 139–158.

Prunet, P., Minster, J.-F., Ruiz-Pino, D., Dadou, I., 1996b. Assimilation of surface data in a one-dimensional physical–biogeochemical model of the surface ocean: 1. Method and preliminary results. Glob. Biogeochem. Cycles 10, 111–138.

Rao, R.R., Molinari, R.L., Festa, J.F., 1989. Evolution of the climatological near-surface thermal structure of the tropical Indian Ocean 1. Description of mean monthly mixed layer depth, and sea surface temperature, surface current, and surface meteorological fields. J. Geophys. Res. 94, 10,801–10,815.

Rix, N.H., 1998. Investigating Indian Ocean variability in a basin scale GCM: Model assessment and model-data intercomparison. PhD thesis, Universität Kiel, 155 pp.

Ryabchenko, V.A., Gorchakov, V.A., Fasham, M.J.R., 1998. Seasonal dynamics and biological productivity in the Arabian Sea euphotic zone as simulated by a three-dimensional ecosystem model. Glob. Biogeochem. Cycles 12, 501–530.

Sarmiento, J.L., Slater, R.D., Fasham, M.J.R., Ducklow, H.W., Toggweiler, J.R., Evans Jr., G.T., 1993. A seasonal three-dimensional ecosystem model of nitrogen cycling in the North Atlantic euphotic zone. Glob. Biogeochem. Cycles 7 (2), 417–450.

Schartau, M., Oschlies, A., Willebrand, J., 2001. Parameter estimates of a zero-dimensional ecosystem model applying the adjoint method. Deep-Sea Res. II 48, 1769–1800.

Shetye, S.R., Gouveia, A.D., Shenoi, S.S.C., 1994. Circulation and

water masses of the Arabian Sea. In: Lal, D. (Ed.), Biogeochemistry of the Arabian Sea. Indian Academy of Sciences, Bangalore, pp. 9–25.

Shi, W., Morrison, J.M., Böhn, E., Manghnani, V., 2000. The Oman upwelling zone during 1993, 1994 and 1995. Deep-Sea Res. II 47, 1227–1247.

Smith, S.L., Codispoti, L.A., Morrison, J.M., Barber, R.T., 1998. The 1994–1996 Arabian Sea Expedition: an integrated, interdisciplinary investigation of the response of the northwestern Indian Ocean to monsoonal forcing. Deep-Sea Res. II 45, 1905–1915.

Stammer, D., Tokmakian, R., Semtner, A., Wunsch, C., 1996. How well does a 1/4° global circulation model simulate large-scale oceanic observations? J. Geophys. Res. 101, 25779–25811.

Stephens, D.P., 1991. The open boundary condition in the United Kingdom Fine-Resolution Antarctic Model. J. Phys. Oceanogr. 21, 1494–1499.

Swathi, P.S., Sharada, M.K., Yajnik, K.S., 2000. A coupled physical–biological–chemical model for the Indian Ocean. Proc. Indian Acad. Sci., A Earth Planet. Sci. 109, 503–537.

Takahashi, T., Wanninkhof, R.H., Feely, R.A., Weiss, R.F., Chipman, D.W., Bates, N.R., Olafsson, J., Sabine, C.L., Sutherland, S.C., 1999. Net sea–air CO_2 flux over the global oceans: an improved estimate based on the air–sea pCO_2 difference. In: Nojiri, Y. (Ed.), Proceedings of the 2nd International Symposium on CO_2 in the Oceans. National Institute for Environmental Studies, Tsukuba, Japan, January 18–23, pp. 9–15.

Tindale, N.W., Pease, P.P., 1999. Aerosols over the Arabian Sea: atmospheric transport pathways and concentrations of dust and sea salt. Deep-Sea Res. II 46, 1577–1595.

Wallcraft, A.J., 1991. The navy layer ocean model users guide. Tech. Rep. 35, Naval Res. Lab., Steniss Space Center.

Ward, B.B., Kilpatrick, K.A., Renger, E.H., Eppley, R.W., 1989. Biological nitrogen cycling in the nitracline. Limnol. Oceanogr. 34, 493–513.

Watts, L.J., Sathyendranath, S., Caverhill, C., Maass, H., Platt, T., Owens, N.J.P., 1999. Modelling new production in the northwest Indian Ocean region. Mar. Ecol. Prog. Ser. 183, 1–12.

Yakushev, E.V., Neretin, L.N., 1997. One-dimensional modeling of nitrogen and sulfur cycles in the aphotic zones of the Black and Arabian seas. Glob. Biogeochem. Cycles 11, 401–414.

Yoshimori, A., Kishi, M.J., 1994. Effects of interaction between two warm-core rings on phytoplankton distribution. Deep-Sea Res. 41, 1039–1052.

Young, D.K., Kindle, J.C., 1994. Physical processes affecting availability of dissolved silicate for diatom production in the Arabian Sea. J. Geophys. Res. 99, 22619–22632.